Construction of Artificial Photosynthetic Reaction Centers on a Protein Surface: Vectorial, Multistep, and Proton-Coupled Electron Transfer for Long-Lived Charge Separation

Yi-Zhen Hu,[†] Shinya Tsukiji,[†] Seiji Shinkai,[†] Shigero Oishi,[‡] and Itaru Hamachi*[,†,§]

Contribution from the Department of Chemistry and Biochemistry, Graduate School of Engineering, Kyushu University, Fukuoka 812-8581, Japan, Department of Chemistry, School of Science, Kitasato University, Sagamihara, Kanagawa 228-8520, Japan, and Institute of Molecular Science, Myodaiji, Okazaki, 444-8585, Japan

Received April 29, 1999. Revised Manuscript Received August 26, 1999

Abstract: Artificial photosynthetic reaction centers have been constructed on a protein surface by cofactor reconstitution, which mimic the function of photosynthetic organisms to convert light energy to chemical potential in the form of long-lived charge-separated states. They feature a ruthenium tris(2,2′-bipyridine) moiety as the sensitizer, which is mechanically linked (i.e., in catenane-type) with a cyclobis(paraquat-*p*-phenylene) unit (BXV^{4+}, acceptor) and covalently linked with a protoheme or Zn−protoporphyrin (donor) located in the myoglobin pocket. Their cofactors **1** and **2**, which are tris(heteroleptic) Ru−bipyridine complexes, were synthesized by sequential coordination of the two different functionalized bipyridine ligands with a readily obtainable precursor $[Ru(4,4'\text{-dimethyl-}2,2'\text{-bipyridine})Cl_3]_n$ followed by metal insertion; this represents a new efficient synthetic method for tris(heteroleptic) Ru(II) complexes of bidentate polypyridine ligands. Reconstitution of apo-myoglobin (Mb) with **1** and **2** affords the two Mb-based artificial triads, $Mb(Fe^{III}OH_2)-Ru^{2+}-BXV^{4+}$ and $Mb(Zn)-Ru^{2+}-BXV^{4+}$. Laser flash photolysis of the $Ru(bpy)_3$ moiety of $Mb(Fe^{III}OH_2)-Ru^{2+}-BXV^{4+}$ in an aqueous solution yields an initial charge-separated state, $Mb(Fe^{III}OH_2)-Ru^{3+}-BXV^{3+\bullet}$, via noncovalent electron transfer, followed by dark electron transfer to generate an intermediate consisting of porphyrin cation radical, $Mb(Fe^{III\bullet}OH_2)-Ru^{2+}-BXV^{3+\bullet}$. $Mb(Fe^{III\bullet}OH_2)-Ru^{2+}-BXV^{3+\bullet}$ thus generated is subsequently converted, via a proton-coupled process and with a quantum yield of 0.005, into the final charge-separated state, $Mb(Fe^{IV}{=}O)-Ru^{2+}-BXV^{3+\bullet}$, which bears an energy more than 1 eV above the ground state and a lifetime ($\tau > 2$ ms) comparable to that of natural photosynthetic reaction center. Photoexcitation of $Mb(Zn)-Ru^{2+}-BXV^{4+}$ also gives rise to a vectorial two-step electron-transfer relay with the intermediate CS state, $Mb(Zn)-Ru^{3+}-BXV^{3+\bullet}$, for the main pathway leading to the final CS state, $Mb(Zn^{+})-Ru^{2+}-BXV^{3+\bullet}$, in a yield of 0.08. Although the driving forces for the recombination of $Mb(Fe^{IV}{=}O)-Ru^{2+}-BXV^{3+\bullet}$ and $Mb(Zn^{+})-Ru^{2+}-BXV^{3+\bullet}$ are similar ($\Delta G \approx 1.30$ eV), the recombination rate of the former is at least 10^2-10^3-fold slower than that of the latter. By analogy with a related system reported previously, it was considered that back ET from $BXV^{3+\bullet}$ to $Mb(Fe^{IV}{=}O)$ might be coupled to the protonation of $Mb(Fe^{IV}{=}O)$ and governed by the slow interconversion between the metal−oxo form and the proton-activated species, rendering the CS state $Mb(Fe^{IV}{=}O)-Ru^{2+}-BXV^{3+\bullet}$ specially long-lived. Control experiments clearly demonstrated that partial incorporation of the triads into the protein matrix plays a crucial role in regulating the electron-transfer pathway and stabilizing the charge separation state.

Introduction

Photoinduced electron transfer to yield long-lived charge-separated (CS) states is the most fundamental energy conversion process of photosynthesis. In photosynthetic bacteria, it is carried out in the photosynthetic reaction center (PRC) by a series of fast and efficient electron-transfer (ET) steps, which move the electron and hole to opposite sides of the biomembrane.[1] The actual photochemistry involves bacteriochlorophylls, bacteriopheophytins, quinones, and other small organic molecules. Primarily, the light induces a charge separation with an electron leaving the special pair of bacteriochlorophylls and passing via intermediates to the primary and secondary quinone acceptors, Q_A and Q_B, respectively. The final ET in PRC between Q_A and Q_B is a proton-coupled process which is assisted by structural changes of the protein matrix.[2] The protein in which multielements of PRC are embedded plays a major role in controlling ET and charge separation. It is generally believed so far that alignment of the electron acceptors within the protein framework of the PRCs spatially separates the photogenerated products, thereby supporting efficient charge separation.[1,3]

Artificial photosynthesis should involve a supramolecular system so as to satisfy many requirements. The key step—as in

* Corresponding author. E-Mail: itarutcm@mbox.nc.kyushu-u.ac.jp.
† Kyushu University.
‡ Kitasato University.
§ Visiting professor at Institute of Molecular Science.

(1) (a) Deisenhofer, J.; Michel, H. *Angew. Chem., Int. Ed. Engl.* **1989**, *28*, 829. (b) Huber, R. *Angew. Chem., Int. Ed. Engl.* **1989**, *28*, 848. (c) Feher, G.; Allen, J. P.; Okamura, M. Y.; Rees, D. C. *Nature* **1989**, *339*, 111.

(2) (a) Kleinfeld, D.; Okamura, M. Y.; Feher, G. *Biochim. Biophys. Acta* **1984**, *766*, 126. (b) Kleinfeld, D.; Okamura, M. Y.; Feher, G. *Biochim. Biophys. Acta* **1985**, *809*, 291.

(3) Kartha, S.; Das, R.; Norris, J. R. *Ions Biol. Syst.* **1991**, *27*, 323.

10.1021/ja991406i CCC: $19.00
Published on Web 12/31/1999

natural photosynthesis—is a vectorial and multistep ET process for long-lived charge separation. Previous research efforts were mainly directed to the syntheses of covalently linked donor−acceptor dyads, triads, tetrads, and pentads.[4,5] The ET products in these systems are stabilized against recombination by their spatial separation in the rigid molecular arrays. Further stabilization of the photogenerated redox products in molecular triads was accomplished by the incorporation of the molecular assemblies into heterogeneous matrixes, such as zeolites or layered phosphates.[6] Structural alignment and rigidification of the molecular arrays in these matrixes result in the suppression of back ET. A significant advance was addressed by Moore and co-workers, in which the excitation of a triad spanning in the bilayer membrane of a liposome generates a pH gradient across the interior and exterior of the liposome, that drives F_0F_1-ATP synthase to produce ATP.[7]

Noncovalently bonded supramolecular assemblies of photosensitizer−acceptor complexes have also been extensively investigated in the past decade.[8] Complementary hydrogen bonds between functionalized photosensitizer and electron acceptors were reported to yield supramolecular dyads.[9] Partially inclusion of donor−acceptor dyads by cyclodextrins was reported to enhance the photoinduced charge separation.[10] Charge-transfer interactions between π-donor and π-acceptor were also utilized for organizing photosensitizer−acceptor dyad and polyad assemblies.[11] Recently, noncovalent and mechanical linkages such as catenane- and rotaxane-modes were elegantly employed to construct artificial photosynthesis models. [12]

We and other groups previously proposed that incorporation of a synthetic dyad into a protein matrix could be an alternative approach for construction of an excellent photochemical system.[13,14] This *semisynthetic approach* is being proven promising by several examples. Reconstitution of apo-hemoproteins (e.g., apomyoglobin (apo-Mb)), for instance, with chemically modified protoporphyrin derivatives having chromophores, donors or acceptors, confers structurally defined donor−acceptor systems.[13] Intermolecular charge separation and the subsequent photocatalytic reactions were elaborately coupled to these systems. Very recently, as an extension of this methodology, we reported semisynthesis of a Mb-based donor−sensitizer−acceptor triad ($Mb(Fe^{III}OH_2)-Ru^{2+}-BXV^{4+}$), in which the acceptor (cyclobis(paraquat-*p*-phenylene) BXV^{4+}) and the sensitizer ($Ru(bpy)_3$) are *noncovalently* linked in a catenane type, and the sensitizer is *covalently* linked with the donor (protoheme) located in the myoglobin pocket (Figures 1 and 2).[15]

This article describes a detailed study on the semisynthesis and photophysics of the Mb-based donor−sensitizer−acceptor triad ($Mb(Fe^{III}OH_2)-Ru^{2+}-BXV^{4+}$. For comparison, another Zn−Mb based triad with similar structure ($Mb(ZnPP)-Ru^{2+}-BXV^{4+}$) is also prepared by cofactor reconstitution. Using these two triads, we clearly understand how a protein matrix is valuable for the construction of a supramolecular ET system. Incorporation of synthetic triads into apo-Mb scaffold affords stabilization of a photogenerated species, as well as regulation of ET pathway. These protein wrapping effects may be ascribed to not only structural extension of the triads, but also an efficient proton-coupling reaction. Photoinduced vectorial, multistep, proton-coupled intraprotein ET can successfully give rise to a very long-lived CS state in a rationally designed semisynthetic protein system.

Results

Molecular Design and Synthesis. We recently reported that photoexcitation of a semisynthetic myoglobin appending $Ru^{2+}(bpy)_3-(Mb(Fe^{III}OH_2)-Ru^{2+}$, Figure 2) in the presence of a sacrificial acceptor ($[Co(NH_3)_5Cl]Cl_2$) generates its oxoferryl

(4) For reviews, see: (a) Gust, D.; Moore, T. A.; Moore, A. L. *Acc. Chem. Res.* **1993**, *26*, 198. (b) Wasielewski, M. L. *Chem. Rev.* **1992**, *92*, 435. (c) Harriman, A.; Sauvage, J. P. *Chem. Soc. Rev.* **1996**, 41. (d) Balzani, V.; Scandola, F. In *Comprehensive Supramolecular Chemistry*; Lehn, J. M., Ed.; Pergamon: Oxford, 1996; Vol. 10, p 687. (e) Collin, J.-P.; Harriman, A.; Heitz, V.; Odobel, F.; Sauvage, J.-P. *Coord. Chem. Rev.* **1996**, *148*, 63.

(5) Recent examples: (a) Zahavy, E.; Seiler, M.; Marx-Tibbon, S.; Joselevich, E.; Willner, I.; Duerr, H.; O'Connor, D.; Harriman, A. *Angew. Chem., Int. Ed. Engl.* **1995**, *34*, 1005. (b) Guldi, D. M.; Maggini, M.; Scorrano, G.; Prato, M. *J. Am. Chem. Soc. 1997*, **119**, 974. (c) Ruthkosky, M.; Kelly, C. A.; Zaros, M. C.; Meyer, G. J. *J. Am. Chem. Soc.* **1997**, *119*, 12004. (d) Wiederrecht, G. P.; Niemczyk, M. P.; Svec, W. A.; Wasielewski, M. R. *J. Am. Chem. Soc.* **1996**, *118*, 81. (e) Liddell, P. A.; Kuciauskas, D.; Sumida, J. P.; Nash, B.; Nguyen, D.; Moore, A. L.; Moore, T. A.; Gust, D. *J. Am. Chem. Soc.* **1997**, *119*, 1400. (f) Osuka, A.; Marumo, S.; Mataga, N.; Taniguchi, S.; Okada, T.; Yamazaki, I.; Nishimura, Y.; Ohno, T.; Nozaki, K. *J. Am. Chem. Soc.* **1996**, *118*, 155. (g) Jolliffe, K. A.; Bell, T. D. M.; Ghiggino, K. P.; Langford, S. J.; Paddon-Row: M. N. *Angew. Chem., Int. Ed.* **1998**, *37*, 916. (h) Kurreck, H.; Huber, M. *Angew. Chem., Int. Ed. Engl.* **1995**, *34*, 849. (i) Gust, D.; Moore, T. A.; Moore, A. L.; Lee, S.-J.; Bittersmann, E.; Luttrull, D. K.; Rehms, A. A.; DeGraziano, J. M.; Ma, X. C.; Gao, F.; Belfored, R. E.; Trier, T. T. *Science* **1990**, *248*, 199.

(6) (a) Vermuelen, L. A.; Thompson, M. E. *Nature* **1992**, *358*, 656. (b) Ungashe, S. B.; Wilson, W. L.; Katz, H. E.; Scheller, G. R.; Putrinski, T. M. *J. Am. Chem. Soc.* **1992**, *114*, 8717. (c) Sykora, M.; Kincaid, J. R. *Nature* **1997**, *387*, 162. (d) Marguerettaz, X.; Redmond, G.; Nagaraja Rao, S.; Fitzmaurice, D. *Chem. Eur. J.* **1996**, *2*, 420.

(7) (a) Steinberg-Yfrach, G.; Liddell, P. A.; Hung, S.-C.; Moore, A. L.; Gust, D.; Moore, T. A. *Nature* **1997**, *385*, 239. (b) Steinberg-Yfrach, G.; Rigaud, J.-L.; Durantini, E. N.; Moore, A. L.; Gust, D.; Moore, T. A. *Nature* **1998**, *392*, 479.

(8) Ward, M. D. *Chem. Soc. Rev.* **1997**, *26*, 365.

(9) (a) Sessler, J. L.; Wang, B.; Harriman, A. *J. Am. Chem. Soc.* **1993**, *115*, 10418. (b) Harriman, A.; Kubo, Y.; Sessler, J. L. *J. Am. Chem. Soc.* **1992**, *114*, 388. (c) Turro, C.; Chang, C. K.; Leroi, G. E.; Cukier, R. I.; Nocera, D. G. *J. Am. Chem. Soc.* **1992**, *114*, 4013. (d) Sun, L.; von Gersdorff, J.; Niethammer, D.; Tian, P.; Kurreck, H. *Angew. Chem., Int. Ed. Engl.* **1994**, *33*, 2318. (e) Sun, L.; von Gersdorff, J.; Sobek, J.; Kurreck, H. *Tetrahedron* **1995**, *21*, 471.

(10) (a) Yonemura, H.; Nakamura, M.; Matsuo, T. *Chem. Phys. Lett.* **1989**, *155*, 157. (b) Yonemoto, E. H.; Kim, Y. I.; Schmehl, R. H.; Wallis, J. O.; Shoulders, B. A.; Richardson, B. R.; Haw, J. F.; Mallouk, T. E. *J. Am. Chem. Soc.* **1994**, *116*, 10557.

(11) (a) Dürr, H.; Bossmann, S.; Kilburg, H.; Trierweiler, H. P.; Schwarz R. In *Frontiers in Supramolecular Organic Chemistry and Photochemistry*; Schneider, H. J., H. Dürr., Eds.; VCH: Weinheim, Germany, 1991; p 453. (b) Seiler, M.; Dürr, H.; Willner, I.; Joselevich, E.; Doron, A.; Stoddart, J. F. *J. Am. Chem. Soc.* **1994**, *116*, 3399. (c) Dürr, H.; Bossmann, S.; Schwarz, R.; Kropf, M.; Hayo, R.; Turro, N. J. *J. Photochem. Photobiol., A* **1994**, *80*, 341. (d) Seiler, M.; Dürr, H. *Liebigs Ann.* **1995**, 407. (e) Kropf, M.; Dürr, H.; Collet, C. *Synthesis* **1996**, 609. (f) Kropf, M.; Joselevich, E.; Dürr, H.; Willner, I. *J. Am. Chem. Soc*. **1996**, *118*, 655. (g) David, E.; Born, R.; Kaganer, E.; Joselevich, E.; Dürr, H.; Willner, I. *J. Am. Chem. Soc*. **1997**, *119*, 7778.

(12) (a) Linke, M.; Chambron, J. C.; Heitz, V.; Sauvage, J.-P. *J. Am. Chem. Soc.* **1997**, *119*, 11329. (b) Chambron, J. C.; Collin, J. P.; Dalbavie, J. O.; Dietrich-Buchecker, C. O.; Heitz, V.; Odobel, F.; Solladie, N.; Sauvage, J.-P. *Coord. Chem. Rev.* **1998**, *180*, 1299. (c) Hu, Y.-Z.; van Loyen, D.; Schwarz, O.; Bossmann, S.; Dürr, H.; Huch, V.; Veith, M. *J. Am. Chem. Soc.* **1998**, *120*, 5822. (d) Hu, Y.-Z.; Bossmann, S.; van Loyen, D.; Schwarz, O.; Dürr, H. *Chem. Eur. J.* **1999**, *5*, 1267.

(13) (a) Hamachi, I.; Tanaka, S.; Shinkai, S. *J. Am. Chem. Soc.* **1993**, *115*, 10458. (b) Hamachi, I.; Tanaka, S.; Tsukiji, S.; Shinkai, S.; Oishi, S. *Inorg. Chem.* **1998**, *37*, 4380. (c) Hamachi, I.; Tsukiji, S.; Tanaka, S.; Shinkai, S. *Chem. Lett.* **1996,** 751. (d) Hamachi, I.; Tsukiji, S.; Shinkai, S.; Oishi, S. *J. Am. Chem. Soc.* **1999**, *121*, 5500. (e) Zahavy, E.; Willner, I. *J. Am. Chem. Soc.* **1996**, *118*, 12499. (f) Willner, I.; Zahavy, E.; Heleg-Shabtai, V. *J. Am. Chem. Soc*. **1995**, *117*, 542. (g) Hayashi, T.; Takimura T.; Ogoshi, H. *J. Am. Chem. Soc.* **1995**, *117*, 11606.

(14) (a) Sakata, Y.; Hirano, Y.; Takemitsu, H.; Misumi, S.; Ochiai, H.; Shibata, H. *Tetrahedron* **1989**, *45*, 4727. (b) Rabanal, F.; Gibney, B. R.; DeGrado W. F.; Moser, C. C.; Dutton, P. L. *Inorg. Chim. Acta* **1996**, *243*, 213-218. (c) Rabanal, F.; DeGrado, W. F.; Dutton, P. L. *J. Am. Chem. Soc.* **1996**, *118*, 473. (d) Robertson, D. E.; Farid, R. S.; Moser, C. C.; Urbauer, J. L.; Mulholland, S. E.; Pidikiti, R.; Lear, J. D.; Wand, A. J.; DeGrado, W. F.; Dutton, P. L. *Nature* **1994**, *368*, 425−431.

(15) Hu, Y.-Z.; Tsukiji, S.; Shinkai, S.; Hamachi, I. *Chem. Lett.* **1999**, 517.

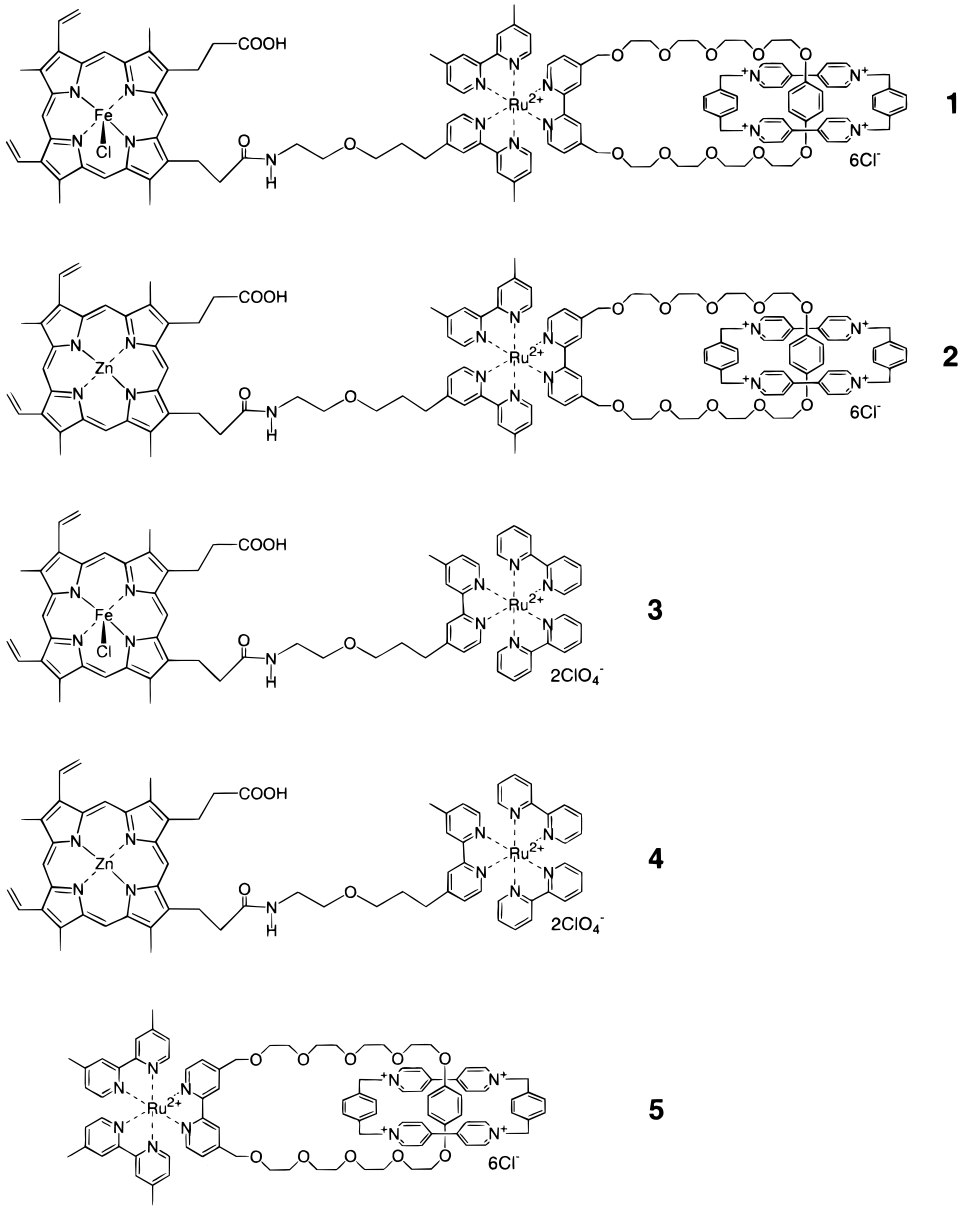

Figure 1. Structures of the triads and dyads studied in this paper.

state (Fe^{IV}═O), so-called compound II, via a intermediate porphyrin radical cation.[13c,d] This success in photogeneration of oxidizing species in the Mb active site prompted us to attempt to attach an electron acceptor to Mb($Fe^{III}OH_2$)−Ru^{2+}, which might thus be photoactivated via intramolecular ET. We chose a viologen derivative as the electron acceptor since its electrochemistry and photochemistry have been well characterized.[11,16] To carry out vectorial electron transfer, the linkage between the sensitizer and the acceptor in the triad should be carefully selected. The CS state lifetimes of covalently linked Ru(bpy)$_3$−viologen systems, unfortunately, are known to be only on the time scale of ps,[17] which are not long enough for the subsequent ET from the heme to the oxidized sensitizer Ru^{3+}(bpy)$_3$ (the first-order rate constant of 7.1×10^5 s^{-1} was determined using the Mb-dyad (Mb($Fe^{III}OH_2$)−Ru^{2+})).[13d] In contrast to these covalently linked analogues, interesting reports showed that the mechanical linkage between the Ru(bpy)$_3$ moiety and the cyclic viologen (BXV^{4+}) in the [2]catenane **5** effectively stabilizes the CS state ($\tau = 517$ ns).[12c,d] Taking these factors into account, a catenane-type mechanical linkage was adopted as the connector between Ru(bpy)$_3$ and viologen, and thus a triad compound (**1**) was rationally designed (Figure 1).

Compounds **1** and **2** bear a tris(2,2′-bipyridine) ruthenium scaffold with three different ligands, i.e., tris(heteroleptic) complexes. Although many synthetic methods of tris(bidentate) ruthenium complexes have been extensively developed, existing procedures are effective only for incorporation of *at most* two different ligands into the coordination sphere. Examples of tris(heteroleptic) complexes are very limited.[18] Here we employ a convenient synthetic method for the tris(heteroleptic) complexes **1** and **2** based on a sequential coordination strategy of the two

(16) (a) Anelli, P. L.; Ashton, P. R.; Ballardini, R.; Balzani, V.; Gandolfi, M. T.; Goodnow, T. T.; Kaifer, A. E.; Philp, D.; Pietraszkiewicz, M.; Prodi, L.; Reddington, M. V.; Slawin, A. M. Z.; Spencer, N.; Stoddart, J. F.; Vicent, C.; Williams, D. J. *J. Am. Chem. Soc*. **1992**, *114*, 193. (b) Asakawa, M.; Ashton, P. R.; Dehaen, W.; L'abbe, G.; Menzer, S.; Nouwen, J.; Raymo, F. M.; Stoddart, J. F.; Tolley, M. S.; Toppet, S.; White, A. J. P.; Williams, D. J. *Chem Eur. J*. **1997**, *3*, 772.

(17) (a) Yonemoto, E. H.; Riley, R. L.; Kim, Y.; J. Atherton, S.; Schmehl, R. H.; Mallouk, T. E. *J. Am. Chem. Soc*. **1992**, *114*, 8081. (b) Yonemoto, E. H.; Saupe, G. B.; Schmehl, R. H.; Hubig, S. M.; Riley, R. L.; Iverson, B. L.; Mallouk, T. E. *J. Am. Chem. Soc*. **1994**, *116*, 4786. (c) Kelly, L.; Rodgers, M. A. J. *J. Phys. Chem*. **1995**, *99*, 13132. (d) Benniston, A. C.; Mackie, P. R.; Harriman, A. *Angew. Chem*. **1998**, *110*, 376.

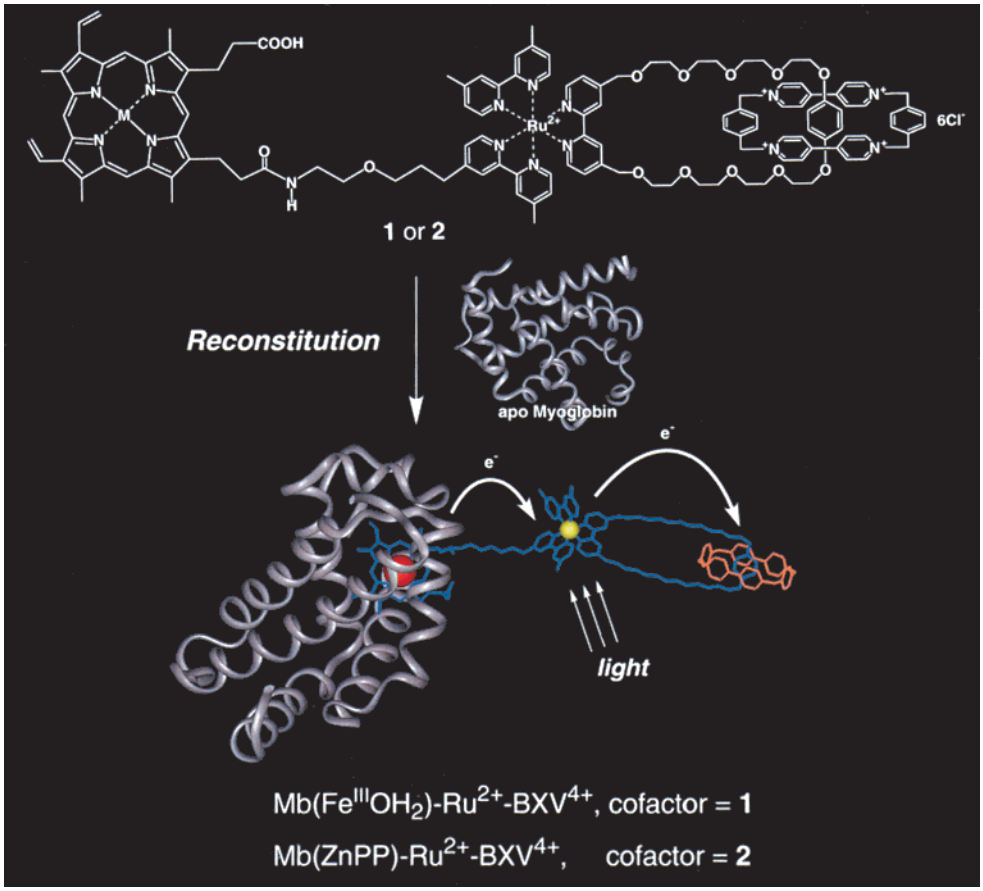

Figure 2. Schematic illustration of the reconstitution of **1** and **2** with apo-myoglobin to afford the myoglobin-based triads, $Mb(Fe^{III}OH_2)-Ru^{2+}-BXV^{4+}$ and $Mb(Zn)-Ru^{2+}-BXV^{4+}$. The structures of the reference myoglobins, $Mb(Fe^{III}OH_2)-Ru^{2+}$ and $Mb(Zn)-Ru^{2+}$ are similar to $Mb(Fe^{III}OH_2)-Ru^{2+}-BXV^{4+}$ and $Mb(Zn)-Ru^{2+}-BXV^{4+}$, but their cofactors are compounds **3** and **4**, respectively.

different polypyridine ligands using [Ru(4,4′-dimethyl-2,2′-bipyridine)Cl_3]$_n$ as a precursor [19,20] (Scheme 1). Reaction of the catenane ligand (**6**)[12d] with [Ru(4,4′-dimethyl-2,2′-bipyridine)-Cl_3]$_n$ [19] affords, after column chromatography on silica gel (eluent: MeOH/2 M NH_4Cl aqueous/$MeNO_2$ = 4/2/3 (v/v/v)) and anion exchange, the catenane complex **7(Cl)$_6$** in 70% yield. Treatment of **7(Cl)$_6$** with the protoporphyrin-tethered bipyridine **8**[13a,b] in ethanol under refluxing, followed by column chromatography on silica gel (eluent: MeOH/2 M NH_4Cl aqueous/$MeNO_2$ = 3/2/3 (v/v/v)) and anion exchange, gives the tris(heteroleptic) complex **9(PF$_6$)$_6$** in 60% yield. Compound **1-(Cl)$_6$** was obtained by iron-insertion of **9(PF$_6$)$_6$** and subsequent anion exchange in 78% yield. Reaction of **9(Cl)$_6$** with $Zn(OAc)_2$ in MeOH at room temperature affords **2(Cl)$_6$** in 95% yield. Four stereoisomers in the Ru coordination sphere may exist in **1** and **2** by this synthetic procedure. These isomers have not been separated in this study.

Reconstitution of the Triads with Apo-Mb. The reconstitution of **1** with apo-Mb (Figure 2) was conducted according to the modified method reported previously by us.[13a,b] To an apo-Mb solution in H_2O was added dropwise 1.4 equiv of **1(Cl)$_6$** dissolved in H_2O (3 mM) in ice-bath. The mixture was incubated at 4 °C, dialyzed against 10 mM KH_2PO_4 buffer (pH 7.0), and then purified by gel chromatography on Sephadex G-25 to afford the triad $Mb(Fe^{III}OH_2)-Ru^{2+}-BXV^{4+}$ in 56% yield.

Spectrophotometric titration of **1** with apo-Mb clearly showed 1:1 complex formation (inset of Figure 3a). The absorption spectrum of the met-form (ferric state, Fe(III)) of $Mb(Fe^{III}OH_2)-Ru^{2+}-BXV^{4+}$ shows a sharp Soret band at 409 nm, a Q-band at 630 nm, a sharp band at 284 nm (LC band of $Ru(bpy)_3$), and a shoulder at 460 nm (MLCT band of $Ru(bpy)_3$) (Figure 3a). This spectrum is nearly identical to the sum of the spectra of native Mb[21] and the BXV^{4+}-catenated $Ru(bpy)_3$ complex (**5**).[12d] Reduction of the met-form of $Mb(Fe^{III}OH_2)-Ru^{2+}-BXV^{4+}$ with $Na_2S_2O_4$ and the subsequent air-oxidation gave absorption spectra corresponding to the deoxy- (434 nm) and oxy- (417, 543, and 582 nm) forms, respectively. These redox properties are essentially identical to those of native Mb and the semisynthetic Mb appending $Ru(bpy)_3$,[13a,b,21] indicating that compound **1** was satisfactorily reconstituted into the heme crevice of apo-Mb.

Reconstitution of **2** with apo-Mb was performed by the same method mentioned above. $Mb(Zn)-Ru^{2+}-BXV^{4+}$ was obtained

(18) (a) Anderson, P. A.; Deacon, G. B.; Haarmann, K. H.; Keene, F. R.; Meyer, T. J.; Reitsma, D. A.; Skelton, B. W.; Strouse, G. F.; Thomas, N. C.; Treadway, J. A.; White, A. H. *Inorg. Chem.* **1995**, *34*, 6145. (b) Rutherford, T. J.; Keene, F. R. *Inorg. Chem.* **1997**, *36*, 2872. (c) Thummel, R. P.; Lefoulon, F.; Chirayil, S. *Inorg. Chem.* **1987**, *26*, 3072. (d) Ross, H. B.;, Boldaji, M.; Rillema, D. P.; Blanton, C. B.; White, R. P. *Inorg. Chem.* **1989**, *28*, 1013. (e) Juris, A.; Campagna, S.; Balzani, V.; Gremaud, G. *Inorg. Chem.* **1988**, *27*, 3652. (f) von Zelewsky, A.; Gremaud, G. *Helv. Chim. Acta* **1988**, *71*, 1108. (g) Black, D. S.; Deacon, G. B.; Thomas, N. C. *Inorg. Chim. Acta* **1982**, *65*, L75. (h) Thomas, N. C.; Deacon, G. B. *Inorg. Synth.* **1989**, *25*, 107. (i) Thomas, N. C.; Deacon, G. B. *Synth. React. Inorg. Met.-Org. Chem.* **1986**, *16*, 85. (j) Black, D. S.; Deacon, G. B.; Thomas, N. C. *Polyhedron* **1983**, *2*, 409. (k) Black, D. S.; Deacon, G. B.; Thomas, N. C. *Aust. J. Chem.* **1982**, *35*, 2445. (l) Strouse, G. F.; Anderson, P. A.; Schoonover, J. R.; Meyer, T. J.; Keene, F. R. *Inorg. Chem.* **1992**, *31*, 3004.

(19) (a) R. A. Krause, *Inorg. Chim. Acta*. **1977**, *22*, 209. (b) Anderson, S.; Seddon, K. R. *J. Chem. Research (S)* **1979**, 74.

(20) We should note that a short communication reported a similar synthetic method for a Ru−tris(diimine) heteroleptic complex, but no detail was described.[18c]

(21) (a) Gibson, Q. H.; Smith, M. H. *J. Physiol.* **1957**, *136*, 27. (b) Chang, C. K.; Traylor, T. G. *Proc. Natl. Acad. Sci. U.S.A.* **1973**, *70*, 2647.

Scheme 1. Synthetic Routes of Triads 1 and 2[a]

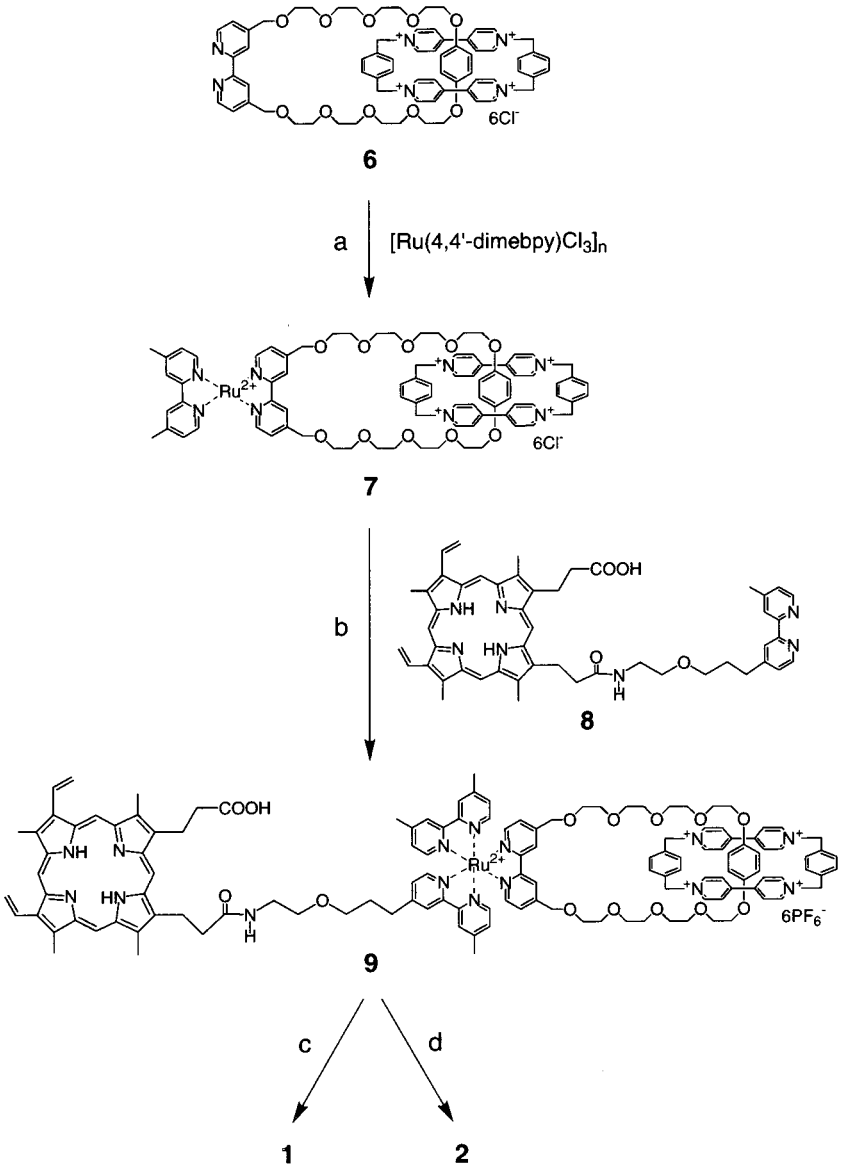

[a] Reagents and conditions: (a) EtOH−H_2O (1:1), reflux under N_2 in the dark, 8 h, 70% yield. (b) EtOH, reflux under N_2 in the dark, 22 h, NH_4PF_6, 60% yield. (c) $FeCl_2 \cdot 4H_2O$, DMF, 65 °C, 8 h, Et_4NCl, 78% yield. (d) $Zn(OAc)_2$, MeOH, rt, 5 h, 95% yield.

in 63% yield after purification. The absorption spectrum of Mb(Zn)−Ru^{2+}−BXV^{4+} shows a sharp Soret band at 428 nm, two Q-bands at 553 and 596 nm, a sharp band at 284 nm (LC of $Ru(bpy)_3$) and a shoulder at 460 nm due to the MLCT band of the $Ru(bpy)_3$ unit (Figure 3b). This spectrum is nearly identical to the sum of the spectra of native Zn−Mb (λ_{max} = 428 nm (Soret band), 553 and 596 nm (Q-bands)) and catenane **5** (λ = 460 nm (MLCT band) and 284 nm (LC band)). Spectrophotometric titration of **2** with apo-Mb quantitatively indicated 1:1 complex formation (inset of Figure 3b). These data confirms the successful reconstitution of **2** with apo-Mb.

Photoinduced Charge Separation in Mb($Fe^{III}OH_2$)−Ru^{2+}−BXV^{4+}. The Mb-based dyad, Mb($Fe^{III}OH_2$)−Ru^{2+}, exhibits weak emission around 630 nm from the $Ru(bpy)_3$ component in buffer solution (pH 7.0). After noncovalent attachment of the acceptor BXV^{4+}, no emission was detected for the triad, Mb($Fe^{III}OH_2$)−Ru^{2+}−BXV^{4+}, indicating that photoinduced ET from $Ru(bpy)_3$ to BXV^{4+} occurs to produce the transient state Mb($Fe^{III}OH_2$)−Ru^{3+}−$BXV^{3+\bullet}$. The redox potential of the oxoferryl-Mb/ferric-Mb couple is +0.896 V vs NHE.[22] Since $Ru^{3+}(bpy)_3$ is a powerful oxidant (+1.245 V vs NHE),[12d] ET from the ferric-Mb to $Ru^{3+}(bpy)_3$ to generate Mb(Fe^{IV}=O)−Ru^{2+}−$BXV^{3+\bullet}$ is thermodynamically favorable.[23] We next examined these possibilities by time-resolved laser flash photolysis.

Figure 4a shows the typical transient absorption spectra after pulsed laser excitation (λ = 355 nm) of Mb($Fe^{III}OH_2$)−Ru^{2+}−BXV^{4+} in buffer (pH 7.0, 50 mM phosphate). For clarity only the spectra at 100 ns and 100 μs are shown in this figure. Figure 5 depicts the relevant high-energy states of Mb($Fe^{III}OH_2$)−Ru^{2+}−BXV^{4+} and some of the pathways available for their interconversion.

Excitation of Mb($Fe^{III}OH_2$)−Ru^{2+}−BXV^{4+} leads to the prompt appearance of two absorption bands at 390 and 610 nm,

(22) He, B.; Sinclair, R.; Copeland, B. R.; Makino, R.; Powers, L. S.; Yamazaki, I. *Biochemistry* **1996**, *35*, 2413.

(23) This has already been confirmed by our intermolecular system using Mb($Fe^{III}OH_2$)−Ru^{2+} in the presence of sacrificial $[Co(NH_3)_5Cl]^{2+}$.[13d] Initially, the excited $Ru^{2+}(bpy)_3$ is oxidatively quenched by $[Co(NH_3)_5Cl]^{2+}$ to produce $Ru^{3+}(bpy)_3$ which then abstracts an electron from the porphyrin ring with a first-order rate constant of 7.1×10^5 s^{-1}. The iron(III) oxidation by the porphyrin radical is followed with concurrent deprotonation to give the oxoferryl state.

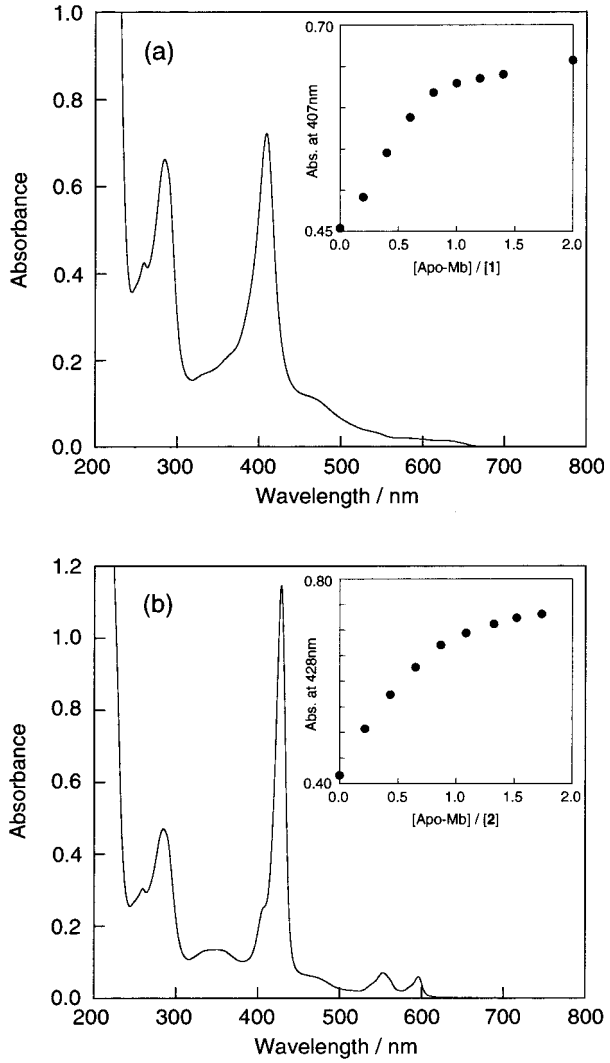

Figure 3. (a) Spectrophotometric titration of **1** with apo-Mb in H_2O. Inset: The titration curve monitored at 408 nm. (b) Absorption spectrum of Mb(Zn)−Ru^{2+}−BXV^{4+} (7 μM) in 50 mM phosphate buffer (pH 7.5). Inset: Spectrophotometric titration curve of **2** with apo-Mb in H_2O.

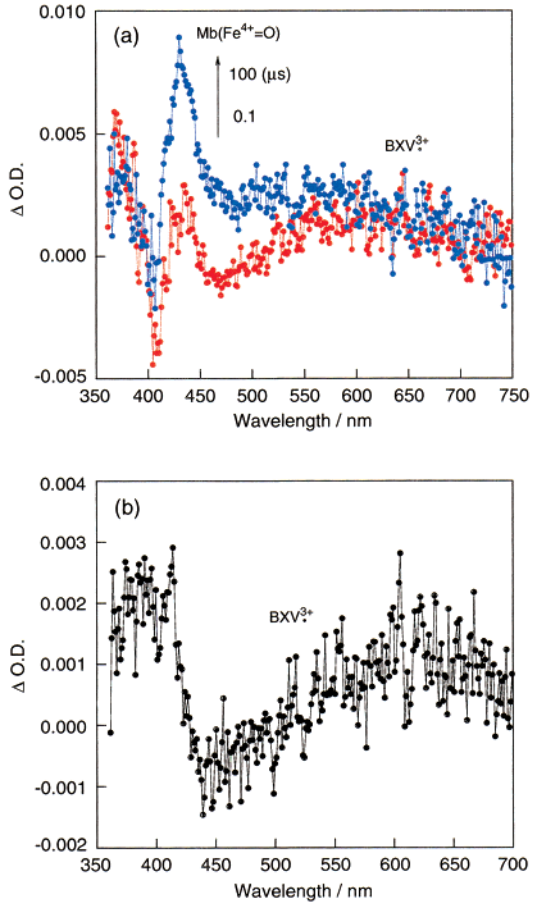

Figure 4. (a) Difference absorption spectra observed after laser excitation (λ = 355 nm) of Mb($Fe^{III}OH_2$)−Ru^{2+}−BXV^{4+} (20 μM) in buffer solution (pH 7.0, 50 mM phosphate) at the following delay times: 100 ns and 100 μs. The sample solutions (3 mL) were degassed with five freeze−pump−thaw cycles before the photolysis. (b) Transient absorption of the compound **1** in the absence of apo-Mb generated by laser excitation at 355 nm at 50 ns delay.

characteristic of the radical cation of bipyridinium salt ($BXV^{3+\bullet}$),[12d] accompanied by the bleaching of the Ru MLCT band (460 nm). This primary spectral change is identical to the results reported for the photolysis of catenane **5** and can be reasonably ascribed to the noncovalent ET between the excited Ru component and BXV^{4+} to yield Mb($Fe^{III}OH_2$)−Ru^{3+}−$BXV^{3+\bullet}$ (step 1 in Figure 5).[12d] The rate of this charge separation is faster than our instrument resolution (fwhm = 5 ns), i.e., $k_1 > 2 \times 10^8$ s^{-1}. Subsequently, bleaching of the Soret band of the Mb($Fe^{III}OH_2$) component and recovery of the Ru MLCT band simultaneously take place in the time range up to 1 μs, concomitantly with the partial decay of the $BXV^{3+\bullet}$ radical absorption which remains constant after the full recovery of the Ru MLCT band. Time traces monitored at 460 nm (MLCT) (Figure 6a) and 610 nm ($BXV^{3+\bullet}$) also clearly show the above changes (data at 610 nm not shown). These spectral changes indicate the competition between the evolution of Mb($Fe^{III}OH_2$)−Ru^{3+}−$BXV^{3+\bullet}$ into the porphyrin cation radical Mb($Fe^{III\bullet}OH_2$)−Ru^{2+}−$BXV^{3+\bullet}$ (step 2 in Figure 5)[13d,24] and its recombination to the ground state (step 4 in Figure 5). Tracing the recovery of the Ru MLCT band (Figure 6a) gave a first-order rate constant of 4×10^6 s^{-1}, which should be the upper limit of the rate constant for the formation of Mb($Fe^{III\bullet}OH_2$)−Ru^{2+}−$BXV^{3+\bullet}$ (step 2). The converted state Mb($Fe^{III\bullet}OH_2$)−Ru^{2+}−$BXV^{3+\bullet}$ is relatively stable [25] and subsequently evolves into a more stable species exhibiting difference absorption bands at 426, 380, and 610 nm in the time range of 1−100 μs (Figure 4a). The difference absorption spectrum of the new species around 426 nm is essentially identical to the difference spectrum between H_2O_2-generated oxoferryl-Mb and ferric-Mb.[13c,d] Thus, the transient absorption spectra obtained after 100 μs can be consistently assigned to the lowest energy charge-separated state Mb(Fe^{IV}=O)−Ru^{2+}−$BXV^{3+\bullet}$ (step 3 in Figure 5).

Monitoring the increase of the absorbance at 426 nm (Figure 6b) gave a first-order rate constant (k_3(app)) of 6.6×10^3 s^{-1} for the conversion of Mb($Fe^{III\bullet}OH_2$)−Ru^{2+}−$BXV^{3+\bullet}$ to Mb(Fe^{IV}=O)−Ru^{2+}−$BXV^{3+\bullet}$ at pH 7.0 (step 3). This conversion is pH-dependent and gradually accelerated with increase of the pH value (Figure 7). As demonstrated previously for the dyad, Mb($Fe^{III}OH_2$)−Ru^{2+},[13c,d] a deprotonated form of the Fe(III) porphyrin cation radical (Mb($Fe^{III\bullet}OH$)) is the active species in the ferryl-Mb formation. This step consists of two protonation/

(24) (a) Low, D. W.; Winkler, J. R.; Gray, H. B. *J. Am. Chem. Soc.* **1996**, *118*, 117. (b) Gans, P.; Buisson, G.; DuÇe, E.; Marchon, J.-C.; Erler, B. S.; Scholz, W. F.; Reed, C. A. *J. Am. Chem. Soc.* **1986**, *108*, 1223.

(25) During the formation of Mb(Fe^{IV}=O)−Ru^{2+}−$BXV^{3+\bullet}$, no appreciable decay of the $BXV^{3+\bullet}$ radical absorption at 610 nm was observed, indicating that the recombination of Mb($Fe^{III\bullet}OH_2$)−Ru^{2+}−$BXV^{3+\bullet}$ to the ground state (step 5 in Figure 5) is negligible.

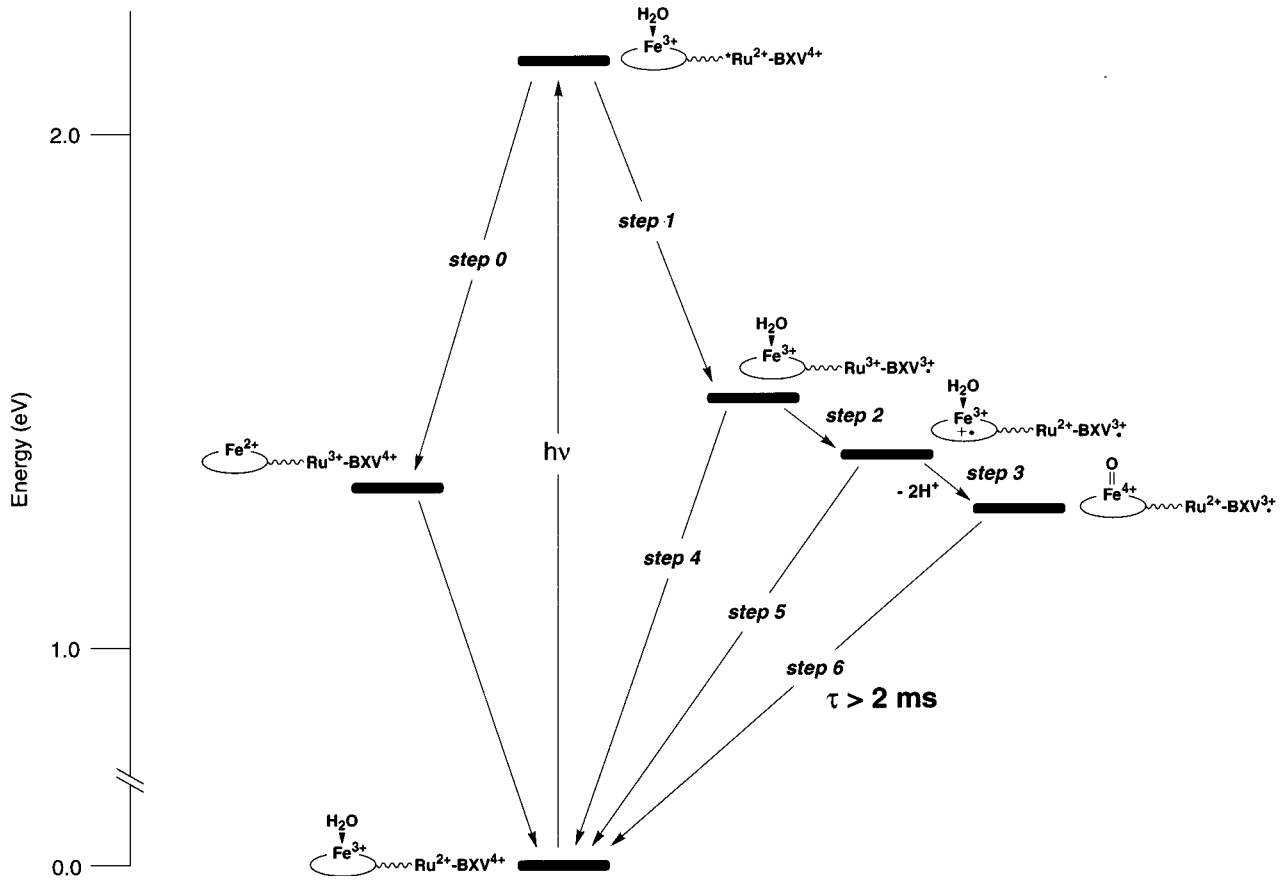

Figure 5. Energetics and selected pathways for Mb($Fe^{III}OH_2$)−Ru^{2+}−BXV^{4+} in buffer solution after excitation to the Ru(bpy)$_3$ excited state. The energy of the excited Ru(bpy)$_3$ component was calculated from the absorption and emission spectra of catenane **5**. The energies of the various charge-separated states were estimated from the corresponding redox potentials of models for the components of Mb($Fe^{III}OH_2$)−Ru^{2+}−BXV^{4+}. The energy levels are not corrected for any Coulombic stabilization of the intermediates.

deprotonation equilibrium and two kinetic constants, that is, p*K*a of the coordinated water of the Fe(III) porphyrin cation radical, p*K*a of a residue of Mb backbone, the conversion rate of Mb(Fe^{III}•OH) into ferry-Mb in the protonated Mb backbone, and the conversion rate in the deprotonated Mb backbone. Thus, step 3 can be described by eqs 1−4:

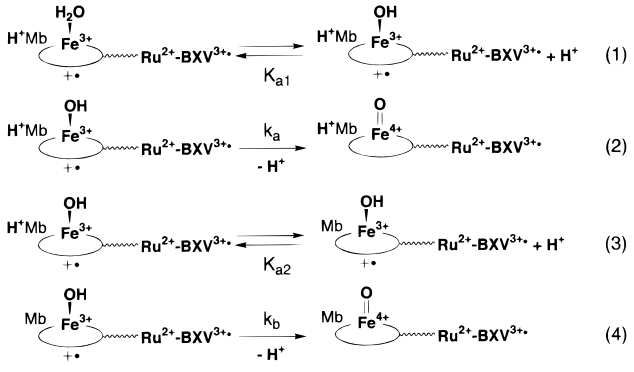

These four equations gave the relationship between the apparent rate constant in step 3 and proton concentration as follows:

$$k_3(\text{app}) = \frac{k_a(K_{a1}K_{a2}[H^+]^2+K_{a2}[H^+]+1) + k_b(K_{a1}[H^+]+1) - k_a}{(K_{a1}[H^+]+1)(K_{a1}K_{a2}[H^+]^2+K_2[H^+]+1)} \quad (5)$$

A simulation curve using eq 5 fits well to the experimental data points, yielding the corresponding values: k_a, k_b, pK_{a1}, and pK_{a2} of 4×10^3 s^{-1}, 3×10^5 s^{-1}, 5.2, and 9.0, respectively. Good agreement of these kinetics with our previous results using Mb($Fe^{III}OH_2$)−Ru^{2+} strongly supports that the ET steps proceed in a manner similar to those of the dyad system.[13c,d]

The kinetic behavior of the final CS state Mb(Fe^{IV}═O)−Ru^{2+}−BXV^{3+}• was monitored at 426 nm (characteristic of the Mb(Fe^{IV}═O) component) and 610 nm (characteristic of the BXV^{3+}• component) as shown in Figure 6c. A rapid increase of BXV^{3+}• and a delayed increase of Mb(Fe^{IV}═O) are fully consistent with the above-mentioned mechanism. After reaching these absorbance maxima, no appreciable decay of Mb(Fe^{IV}═O)−Ru^{2+}−BXV^{3+}• occurs in the time range detected (up to 2 ms) at both 426 and 610 nm. Unfortunately, the precise determination of the lifetime of Mb(Fe^{IV}═O)−Ru^{2+}−BXV^{3+}• failed because of the instrumental limitation. However, we conclude that it is at least longer than 2 ms.

Next, control experiments with compound **1** were conducted in the absence of the protein matrix in order to investigate protein effects. Pulsed laser excitation of **1** without apo-Mb in aqueous solution results in the prompt appearance of the BXV^{3+}• radical monitored at 390 and 610 nm and the bleaching of the Ru MLCT band (460 nm), corresponding to the formation of the CS state, Fe^{III}(Cl)−Ru^{3+}−BXV^{3+}• (Figure 4b). However, the BXV^{3+}• radical absorption rapidly decays within 1 μs, accompanied by the recovery of the Ru MLCT band, implying the recombination of Fe^{III}(Cl)−Ru^{3+}−BXV^{3+}• to the ground state. It is clear that a multistep ET does not occur without Mb, in sharp contrast to the Mb-based triad.

The quantum yield of Mb(Fe^{IV}═O)−Ru^{2+}−BXV^{3+}• was determined by a comparative method using the triplet state of

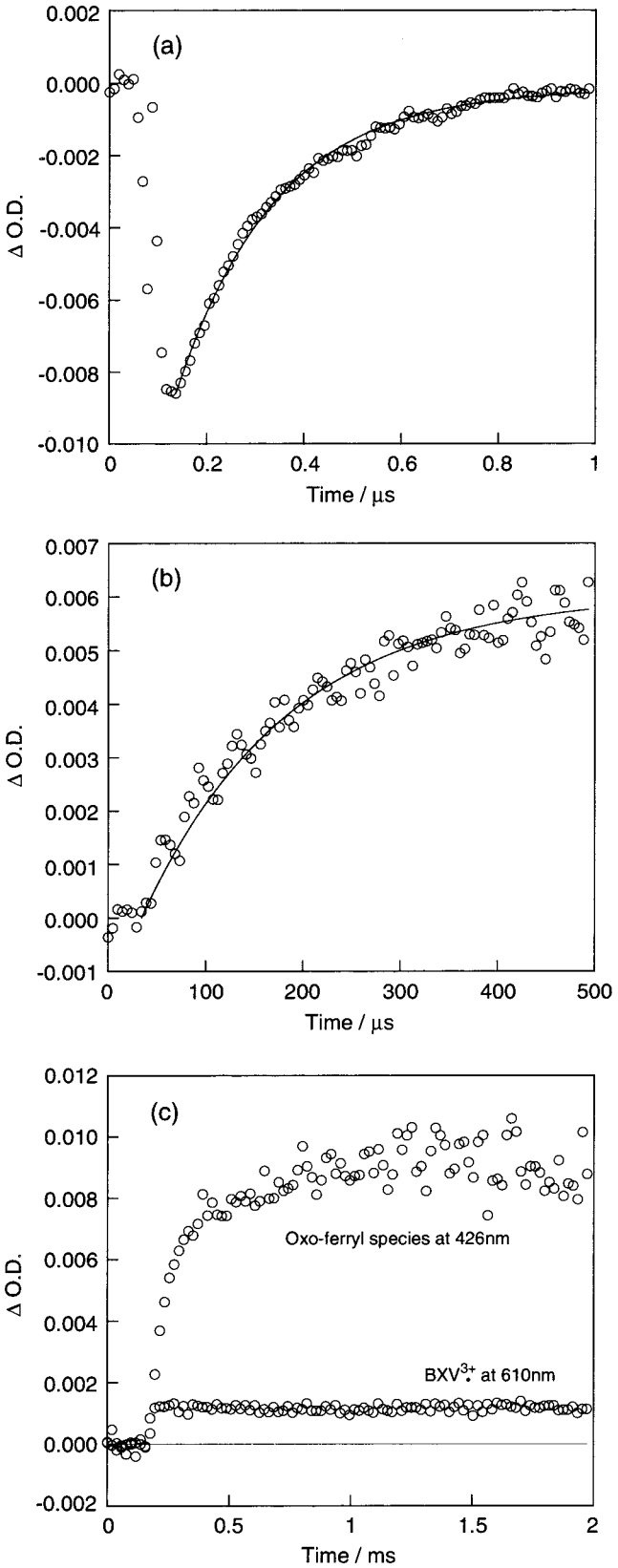

Figure 6. (a) Kinetic trace for the recovery of the MLCT band of the $Ru(bpy)_3$ unit at 460 nm. (b) Transient absorption kinetic trace in the time range up to 500 μs monitored at 426 nm. (c) Transient absorption kinetics in the time range up to 2 ms monitored at 426 and 610 nm. The solid lines in (a) and (b) show the fitting curves which obey the first-order kinetics of the single component. The species giving rise to the transient in (c) is ascribed to the charge-separated state, $Mb(Fe^{IV}{=}O){-}Ru^{2+}{-}BXV^{3+\bullet}$. All of the experiments were performed by laser flash excitation of a degassed buffer solution of $Mb(Fe^{III}OH_2){-}Ru^{2+}{-}BXV^{4+}$ (20 μM) at 355 nm.

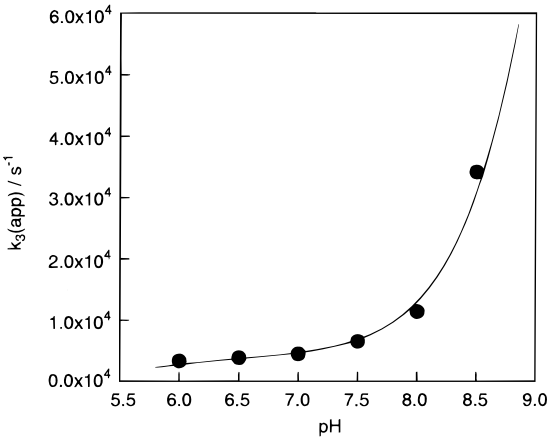

Figure 7. pH dependence of the rate of the $Mb(Fe^{IV}{=}O){-}Ru^{2+}{-}BXV^{3+\bullet}$ formation from the porphyrin radical $Mb(Fe^{III\bullet}OH_2){-}Ru^{2+}{-}BXV^{3+\bullet}$. Study at pH value higher than 8.0 was prevented by the decomposition of the protein. The fitting curve is given by the solid line.

benzophenone[26] as an external standard. Since the absorption of the $Mb(Fe^{III}OH_2)$ and $Ru^{2+}(bpy)_3$ components overlaps with each other and only the light-absorption by the $Ru^{2+}(bpy)_3$ moiety is effective for ET, the quantum yield of the final CS state will vary depending on excitation wavelength. Excitation of a solution of $Mb(Fe^{III}OH_2){-}Ru^{2+}{-}BXV^{4+}$ at 355 nm, produces $Mb(Fe^{IV}{=}O){-}Ru^{2+}{-}BXV^{3+\bullet}$ in a quantum yield of $\Phi_1 = 0.005$, based on the absorption of $Ru^{2+}(bpy)_3$. This relatively low quantum yield might be explained by two factors. First, the oxidative quenching of the excited $Ru^{2+}(bpy)_3$ moiety by the heme (step 0 in Figure 5), i.e., $Mb(Fe^{III}OH_2){-}{}^{*}Ru^{2+}{-}BXV^{4+} \rightarrow Mb(Fe^{II}){-}Ru^{3+}{-}BXV^{4+}$,[13a,b] considerably competes with the photooxidation of $^{*}Ru^{2+}(bpy)_3$ by the BXV^{4+} unit (step 1 in Figure 5). In addition, the evolution of $Mb(Fe^{III}OH_2){-}Ru^{3+}{-}BXV^{3+\bullet}$ into $Mb(Fe^{III\bullet}OH_2){-}Ru^{2+}{-}BXV^{3+\bullet}$ (step 2 in Figure 5) is slower than its recombination to the ground state (step 4 in Figure 5). Combination of these two factors leads to the rather lower yield of $Mb(Fe^{IV}{=}O){-}Ru^{2+}{-}BXV^{3+\bullet}$.

Photoinduced Charge Separation in $Mb(Zn){-}Ru^{2+}{-}BXV^{4+}$. With the aim of exploring the protein matrix effects, we studied photophysics of zinc-substituent (Mb(**2**)) and compared it to the iron-centered triad Mb(**1**). The most significant difference between Mb(**1**) and Mb(**2**) is the coordination sphere of the metal center of the heme site, that is, iron(III) is coordinated to H_2O at the sixth coordination site, whereas the sixth site of zinc(II) is vacant.

Under the same conditions, the shapes and intensities of the emission spectra of $Mb(Zn){-}Ru^{2+}{-}BXV^{4+}$, $Mb(Zn){-}Ru^{2+}$ and Zn−Mb are very similar (Figure 8a), indicating that quenching of the fluorescence from the Zn−protoporphyrin (ZnPP) unit of $Mb(Zn){-}Ru^{2+}{-}BXV^{4+}$ does not occur. Therefore, within $Mb(Zn){-}Ru^{2+}{-}BXV^{4+}$, ET from the excited singlet state of ZnPP to the $Ru(bpy)_3$ or BXV^{4+} site can be ruled out.

We then checked the excitation spectra of $Mb(Zn){-}Ru^{2+}{-}BXV^{4+}$ and $Mb(Zn){-}Ru^{2+}$ at emission wavelength of 596 nm. Figure 8b displays that the absorption peaks of both the ZnPP and $Ru(bpy)_3$ units are reproduced in the excitation spectrum of $Mb(Zn){-}Ru^{2+}$ (428 and 556 nm for ZnPP and 460 nm for $Ru(bpy)_3$), indicating that the emission of $Ru(bpy)_3$ is buried in the ^{1}ZnPP fluorescence spectrum (Figure 8a). However, in the case of $Mb(Zn){-}Ru^{2+}{-}BXV^{4+}$, only the ZnPP absorption peaks are reproduced in the excitation spectrum. No absorption

(26) Bonneau, R.; Carmichael, I.; Hug, G. *Pure Appl. Chem.* **1991**, *63*, 289.

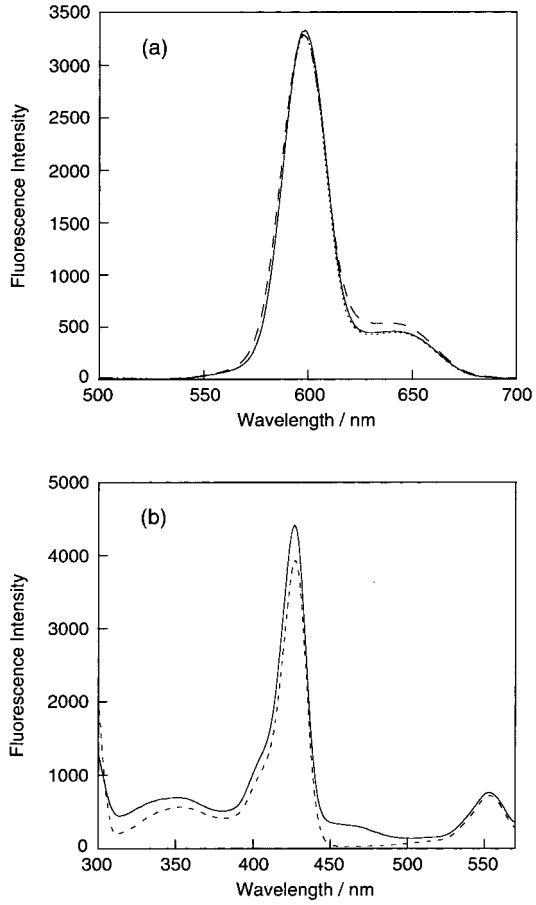

Figure 8. (a) Comparison of the emission spectra of Mb(Zn)−Ru^{2+}−BXV^{4+}, Mb(Zn)−Ru^{2+} and Zn−Mb in 10 mM phosphate buffer. Excitation wavelength: 428 nm. Dashed line: Zn−Mb; solid line: Mb(Zn)−Ru^{2+}; dotted line: Mb(Zn)−Ru^{2+}−BXV^{4+}. Concentrations for the three samples were adjusted to the same (1 μM). (b) Excitation spectra of Mb(Zn)−Ru^{2+}−BXV^{4+} and Mb(Zn)−Ru^{2+} in 10 mM phosphate buffer (pH 7.0). Solid line: Mb(Zn)−Ru^{2+}; dashed line: Mb(Zn)−Ru^{2+}−BXV^{4+}. Emission wavelength detected is 596 nm.

peak from the $Ru(bpy)_3$ unit (460 nm) is observed, suggesting that the $Ru(bpy)_3$ emission is completely quenched. Quenching of the $Ru(bpy)_3$ emission strongly supports that photoinduced ET from the excited $Ru(bpy)_3$ to BXV^{4+} takes place in Mb(Zn)−Ru^{2+}−BXV^{4+}, leading to the formation of the CS state, Mb(Zn)−Ru^{3+}−$BXV^{3+\bullet}$.

On the basis of the steady state photochemical studies, the energy levels of the locally excited state of the $Ru^{2+}(bpy)_3$ component, the hypothetical ion-pair states of Mb(Zn)−Ru^{2+}−BXV^{4+}, and the pathways available for their interconversion are depicted as Figure 9. The energies of ion-pair states are estimated from the sum of the one-electron oxidation and reduction potentials, that is, the one-electron oxidation potentials of Zn−Mb and $Ru(bpy)_3$ are 1.06 V[27] and 1.245 V vs NHE, respectively,[12d] and the one-electron reduction potential of BXV^{4+} is −0.213 V vs NHE.[12d] An energetically important feature is as follows: an energy gradient exists for Mb(Zn)−Ru^{2+}−BXV^{4+} in the order of Mb(Zn)−$^{*}Ru^{2+}$−BXV^{4+} > Mb(Zn)−Ru^{3+}−$BXV^{3+\bullet}$ > Mb(Zn^{+})−Ru^{2+}−$BXV^{3+\bullet}$, which may allow a stepwise ET relay of Mb(Zn)−$^{*}Ru^{2+}$−BXV^{4+} → Mb(Zn)−Ru^{3+}−$BXV^{3+\bullet}$ → Mb(Zn^{+})−Ru^{2+}−$BXV^{3+\bullet}$ (steps 1 and 2 in Figure 9). Detailed mechanisms were next investigated by time-resolved laser photolysis studies.

For simplification of analysis, the $Ru^{2+}(bpy)_3$ component of Mb(Zn)−Ru^{2+}−BXV^{4+} was selectively excited in the laser flash photolysis experiments. The excitation wavelength used was 460 nm, where more than 90% of the light is absorbed by the $Ru^{2+}(bpy)_3$ moiety (MLCT band) and less than 10% by the ZnPP moiety. As shown in Figure 10a, after pulsed laser excitation of Mb(Zn)−Ru^{2+}−BXV^{4+}, absorption bands at 385 nm, 470 nm, 610 nm (shoulder) and 670 nm promptly appear, accompanied by the bleaching of Soret and Q-bands (428, 553, and 596 nm). According to the literatures[27,28] the absorption band at 470 nm can be assigned to the triplet state, ^{3}ZnPP, which was generated by the weak light absorption by the ZnPP moiety at 460 nm. The peak at 385 nm and the shoulder at 610 nm are characteristic of the radical cation of bipyridinium salt (i.e., $BXV^{3+\bullet}$),[12d] and the band centered at 670 nm is characteristic of $ZnPP^{+}$,[29] which partially overlaps with the absorption of the $BXV^{3+\bullet}$ radical. The appearance of $BXV^{3+\bullet}$ and $ZnPP^{+}$ clearly implies the formation of the CS state, i.e., Mb(Zn^{+})−Ru^{2+}−$BXV^{3+\bullet}$. The absorption bands of ^{3}ZnPP, $BXV^{3+\bullet}$, and $ZnPP^{+}$ species decay completely within 50 μs, concomitantly with the recovery of the Soret and Q- bands of ZnPP. Laser excitation of Zn−Mb or Mb(Zn)−Ru^{2+} under the same conditions simply produced the absorption of their ZnPP triplet states (^{3}Zn−Mb or Mb(^{3}Zn)−Ru^{2+}), and any other transient absorption was not detected.

The lifetime of Mb(^{3}Zn)−Ru^{2+} was determined to be 3.9 ms by monitoring the decay at 470 nm, whereas Mb(^{3}Zn)−Ru^{2+}−BXV^{4+} decays biexponentially with lifetimes of 2.1 μs (70%) and 19.8 μs (30%).[30] Apparently, the decay of Mb(^{3}Zn)−Ru^{2+}−BXV^{4+} is much faster than that of Mb(^{3}Zn)−Ru^{2+} and ^{3}Zn−Mb. Either energy transfer or ET from ^{3}ZnPP to $Ru(bpy)_3$ is energetically unfavorable ($E(Ru^{2+}/Ru^{+}) = -1.39$ vs NHE).[12d] Thus, the quenching of Mb(^{3}Zn)−Ru^{2+}−BXV^{4+} is reasonably attributable to the direct, long-distance ET from ^{3}ZnPP to BXV^{4+}, i.e., Mb(^{3}Zn)−Ru^{2+}−BXV^{4+} → Mb(Zn^{+})−Ru^{2+}−$BXV^{3+\bullet}$ and the rate constants for this ET process were calculated to be 4.8×10^{5} s^{-1} and 5.0×10^{4} s^{-1} using the lifetimes of Mb(^{3}Zn)−Ru^{2+}−BXV^{4+} and Mb(^{3}Zn)−Ru^{2+}.

The kinetic behavior of the CS state, Mb(Zn^{+})−Ru^{2+}−$BXV^{3+\bullet}$, was monitored at 385 nm (Figure 10b). The time course shows that Mb(Zn^{+})−Ru^{2+}−$BXV^{3+\bullet}$ is formed immediately after the laser flash and then decays slowly within 100 μs. Monitoring at 670 nm yielded similar results. The rate for the formation of Mb(Zn^{+})−Ru^{2+}−$BXV^{3+\bullet}$ is faster than our instrument resolution (fwhm = 5 ns, i.e., $k_{cs} > 2 \times 10^{8}$ s^{-1}). This rate is over 500 times faster than the decay of Mb(^{3}Zn)−Ru^{2+}−BXV^{4+} ($\tau = 2.1$ μs), indicating that the contribution of the direct ET pathway, i.e., Mb(^{3}Zn)−Ru^{2+}−BXV^{4+} → Mb(Zn^{+})−Ru^{2+}−$BXV^{3+\bullet}$, to the formation of the CS state is negligible. Therefore, it is reasonably concluded that the CS state is generated via the stepwise ET route shown in Figure 9, i.e., Mb(Zn)−$^{*}Ru^{2+}$−BXV^{4+} → Mb(Zn)−Ru^{3+}−$BXV^{3+\bullet}$ → Mb(Zn^{+})−Ru^{2+}−$BXV^{3+\bullet}$ (steps 1 and 2), the rate constants of which are both faster than 2×10^{8} s^{-1}.

(27) (a) Axup, A. W.; Albin, M.; Mayo, S. L.; Crutchley, R. J.; Gray, H. B. *J. Am. Chem. Soc*. **1988**, *110*, 435. (b) Stanford, M. A.; Hoffman, B. M. *J. Am. Chem. Soc*. **1981**, *103*, 4104.

(28) (a) Zemel, H.; Hoffman, B. M. *J. Am. Chem. Soc*. **1981**, *103*, 1192. (b) Barboy, N.; Feitelson, J. *Biochemistry* **1987**, *26*, 3240.

(29) (a) Liang, N.; Mauk, A. G.; Pielak, G. J.; Johnson, J. A.; Smith, M.; Hoffman, B. M. *Science* **1988**, *240*, 311. (b) Nocek, J. M.; Sishta, B. P.; Cameron, J. C.; Mauk, A. G.; Hoffman, B. M. *J. Am. Chem. Soc*. **1997**, *119*, 2146.

(30) The lifetime of Mb(^{3}Zn)−Ru^{2+} is slightly shorter than that of ^{3}Zn−Mb (15 ms) under the same conditions,[27,28] which might arise from the structure perturbation by the appended $Ru(bpy)_3$ unit. The two lifetimes of Mb(^{3}Zn)−Ru^{2+}−BXV^{4+} can be assigned to the triplet states of the conformers of Mb(Zn)−Ru^{2+}−BXV^{4+} with alternative distances between the BXV^{4+} unit and ZnPP, which originate from the mechanical linkage (vide infra).

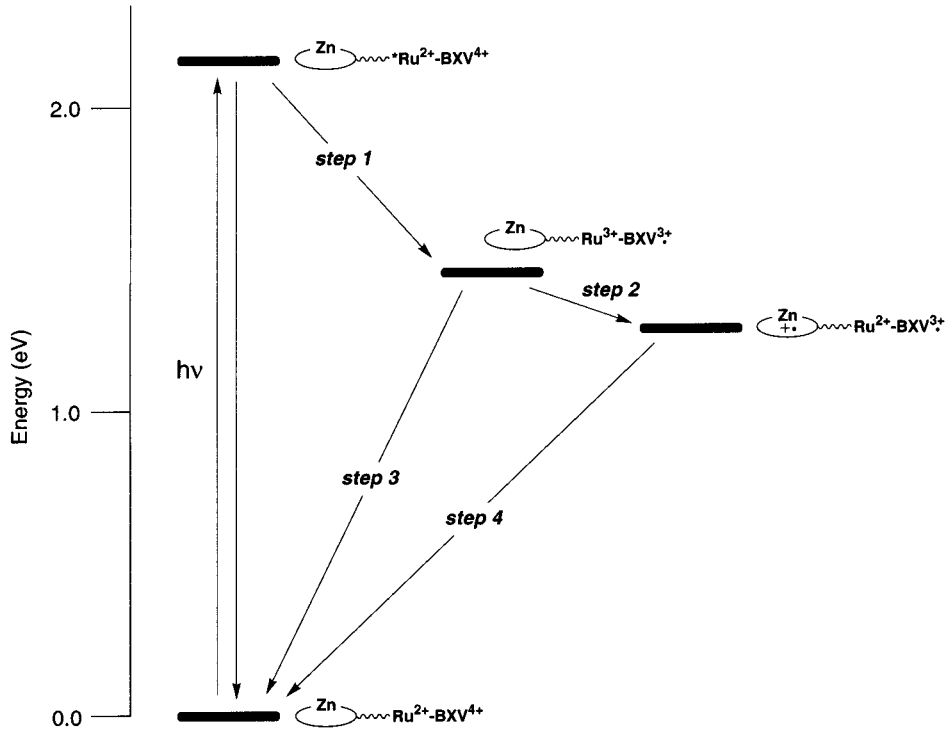

Figure 9. Energy levels of the locally excited state of the $Ru^{2+}(bpy)_3$ moiety and the hypothetical ion-pair states of $Mb(Zn)-Ru^{2+}-BXV^{4+}$ and the pathways available for their interconversion. For comparison purpose, the excited states of ZnPP are not present.

Figure 10b shows that the generated $Mb(Zn^{+})-Ru^{2+}-BXV^{3+\bullet}$ decays via its charge recombination (step 4 in Figure 9). Analysis of the decay curve yields a biexponential fit with lifetimes of 1.1 μs (75%) and 18.4 μs (25%), which lead to rate constants k_4' for the back ET of 9.1×10^5 s^{-1} and 5.4×10^4 s^{-1}. The biphasic decay is quite similar to that of compound **5** reported previously,[12d] in which this behavior was attributed to the catenane-mode of the mechanical linkage between $Ru(bpy)_3$ and BXV^{4+}. Some conformers with different donor−acceptor distances might exist due to the mechanical linkage. Accordingly, the two lifetimes can be assigned to back ET from the reduced viologen to the oxidized heme center in these conformers of $Mb(Zn)-Ru^{2+}-BXV^{4+}$ with alternative distances between the BXV^{4+} unit and ZnPP. We also investigated pH dependence of the photophysical properties of $Mb(Zn)-Ru^{2+}-BXV^{4+}$ in the pH range of 6.0−8.0. In contrast to the case of $Mb(Fe^{III}OH_2)-Ru^{2+}-BXV^{4+}$, change of the pH value shows no obvious effect on the photophysics of $Mb(Zn)-Ru^{2+}-BXV^{4+}$.

A quantum yield for the generation of $Mb(Zn^{+})-Ru^{2+}-BXV^{3+\bullet}$ irradiated at the MLCT band of the Ru component is estimated to be $\Phi_2 = 0.08$, which is much higher than that of $Mb(Fe^{IV}{=}O)-Ru^{2+}-BXV^{3+\bullet}$ ($\Phi_1 = 0.005$ based on the absorption of Ru component, see above). The great improvement of the quantum yield is mainly attributable to the fact that the oxidative quenching of the excited $Ru(bpy)_3$ by metallo-PP (step 0 in Figure 5) is completely inhibited for $Mb(Zn)-Ru^{2+}-BXV^{4+}$, as well as the accelerated reduction of $Ru^{3+}(bpy)_3$ by ZnPP (step 2).

In the absence of the protein matrix, the photophysics of compound **2** is much different from that of $Mb(Zn)-Ru^{2+}-BXV^{4+}$. Without apo-Mb, **2** exhibits weak fluorescence with λ_{max} at 596 and 649 nm (shoulder), the fluorescence quantum yield of which is ~90 times lower than that of Zn-protoporphyrin IX (the parent) and $Mb(Zn)-Ru^{2+}-BXV^{4+}$, suggesting the efficient ET from the excited singlet state, ^{1}ZnPP, to the BXV^{4+} moiety. These fluorescence behaviors show good agreement with the preliminary molecular modeling of **2**, in which a U-shaped conformation of **2** without protein matrix is suggested.[31] Without apo-Mb, the ZnPP and BXV^{4+} unit are close each other so as to quench ^{1}ZnPP efficiently by BXV^{4+}. Great recovery of the fluorescence of ZnPP in $Mb(Zn)-Ru^{2+}-BXV^{4+}$ indicates that the U-shaped conformation changes to a more extended one by incorporation of the heme unit of **2** into the apo-Mb matrix so that ^{1}ZnPP is not quenched by BXV^{4+}. Laser excitation (460 nm) of **2** produces promptly a CS state ($ZnPP^{+}-Ru^{2+}-BXV^{3+\bullet}$) having a lifetime of 300 ns, which is much shorter than that of $Mb(Zn^{+})-Ru^{2+}-BXV^{3+\bullet}$.

Discussion

Two triads (**1** and **2**), both of which bear a tris(heteroleptic) Ru−polypyridine complex moiety, were successfully synthesized by a convenient method, i.e., stepwise addition of two different polypyridine ligands with a readily obtainable precursor $[Ru(4,4'\text{-dimethyl-}2,2'\text{-bipyridine})Cl_3]_n$. Recently, Keene and coworkers reported a synthetic method for heteroleptic tris(bidentate) ruthenium complex using the sequential addition of the polypyridyl ligands to $[Ru(CO)_2Cl_2]_n$ (5 steps).[18a,b] This method, however, needs a strong oxidant, trimethylamine *N*-oxide (TMNO), for the decarbonylation, which limits its application to the synthesis of Ru complexes bearing oxidation-sensitive moieties such as protoporphyrin IX and BXV^{4+} cyclophane. Compared with Keene's method, it is clear that the present one bears the advantages of milder reaction conditions, simpler procedures and higher yield. Thus, the synthetic technique described here provides an efficient and general route for the preparation of bis(heteroleptic) and tris(heteroleptic) Ru(II) complexes.

Reconstitution of **1** and **2** with apo-Mb afforded two protein-based artificial reaction centers, $Mb(Fe^{III}OH_2)-Ru^{2+}-BXV^{4+}$ and $Mb(Zn)-Ru^{2+}-BXV^{4+}$. To the best of our knowledge,

(31) Hu, Y.-Z.; Takashima, H.; Tsukiji, S.; Shinkai, S.; Nagamune, T.; Oishi, S.; Hamachi, I. *Chem. Eur. J.*, in press.

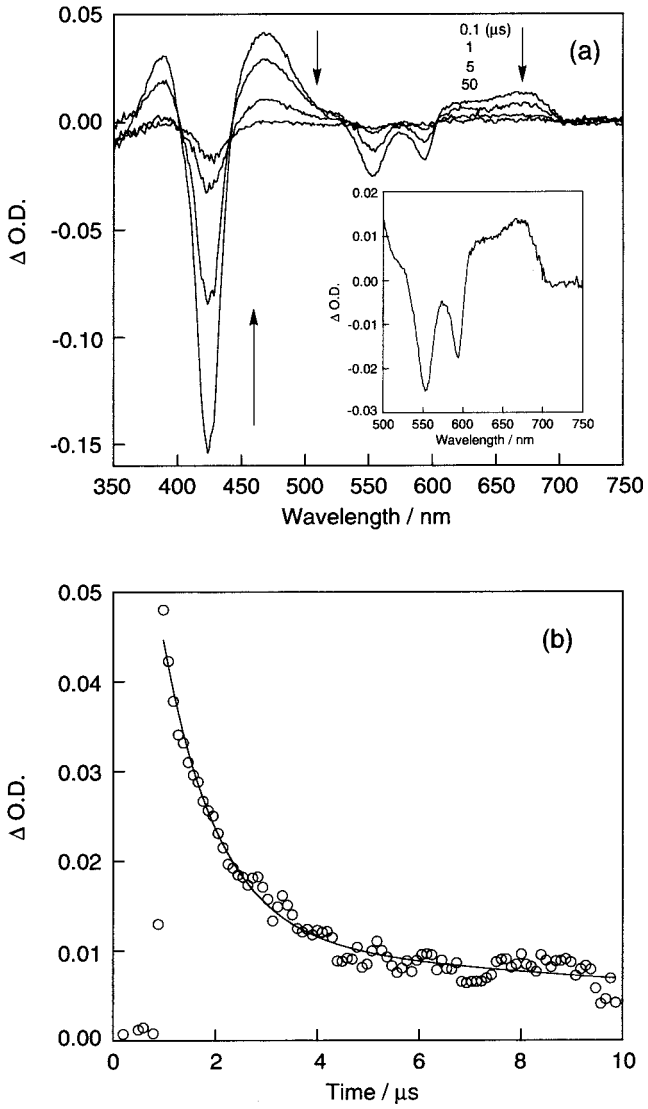

Figure 10. (a) Excited state difference absorption spectra observed after laser excitation ($\lambda = 460$ nm) of Mb(Zn)−Ru^{2+}−BXV^{4+} (8.0 μM) in buffer solution (pH 7.0, 50 mM phosphate buffer) at the following delay times: 100 ns, 1 μs, 5 μs, and 50 μs. Inset: Expansion of the region between 500 and 750 nm (100 ns) (b) Transient absorption kinetics in the time range of up to 10 μs monitored at 385 nm after laser flash excitation of a degassed buffer solution (pH 7.0, 50 mM phosphate buffer) containing Mb(Zn)−Ru^{2+}−BXV^{4+} (8.0 μM) at 460 nm. The fitting curve is given by the solid line.

these are first examples of protein-based semisynthetic triads. The kinetic and steady-state spectroscopic data reveal a vectorial two-step ET relay with the intermediate CS state, Mb($Fe^{III}OH_2$)−Ru^{3+}−$BXV^{3+\bullet}$ or Mb(Zn)−Ru^{3+}−$BXV^{3+\bullet}$, for the main pathway leading to the long-lived CS states. In the case of Mb($Fe^{III}OH_2$)−Ru^{2+}−BXV^{4+}, the stepwise ET is followed by a proton-coupled conversion of the porphyrin radical cation into oxoferryl species, i.e., the final CS state (Mb-(Fe^{IV}=O)−Ru^{2+}−$BXV^{3+\bullet}$), the energy level of which was estimated to be ~1.3 eV, ignoring work terms, as the difference between the heme and the BXV^{4+} redox potentials. It is noteworthy that upon photoexcitation, over 50% of the primary excited-state energy (2.16 eV of Mb($Fe^{III}OH_2$)−$^*Ru^{2+}$−BXV^{4+}) is stored in the final CS state for a lifetime longer than 2 ms, which is comparable to the value of natural PRCs. On the other hand, the photoinduced charge separation and recombination of Mb(Zn)−Ru^{2+}−BXV^{4+} are pH-independent.

In the absence of a protein matrix, compounds **1** and **2** exhibit much different photochemical behaviors from their Mb-based counterparts.[31] Photoexcitation of **1** only generates a short-lived CS state, Fe^{III}(Cl)−Ru^{3+}−$BXV^{3+\bullet}$, and any iron-related transient species was not observed, in sharp contrast to the case of Mb-($Fe^{III}OH_2$)−Ru^{2+}−BXV^{4+}. In compound **2**, direct ET from the excited singlet state of ZnPP to BXV^{4+} is the dominant ET pathway, and the CS state decays much faster than Mb(Zn^+)−Ru^{2+}−$BXV^{3+\bullet}$. Therefore, it is clear that partial fixation of the chromophore in a protein matrix not only regulates the vectorial, multistep ET pathway but also stabilizes the CS state to a large extent in both Mb($Fe^{III}OH_2$)−Ru^{2+}−BXV^{4+} and Mb(Zn)−Ru^{2+}−BXV^{4+}. Steady-state fluorescence and molecular modeling studies of compound **2** strongly suggest that a U-shape-like conformation of **2** changes to a more expanded form by its incorporation into apo-Mb. Conceivably, similar to natural PRC, incorporation of the cofactors into the protein scaffold spatially separates the photogenerated products, thereby avoiding the fast charge recombination.

Although the driving forces for the recombination of Mb-(Fe^{IV}=O)−Ru^{2+}−$BXV^{3+\bullet}$ and Mb(Zn^+)−Ru^{2+}−$BXV^{3+\bullet}$ are similar ($\Delta G \cong 1.3$ eV), the recombination rate of the former is at least 10^2−10^3-fold slower than that of the latter. Similar results have been reported for the comparison between ET in a_5Ru^{II}(His48)-attached Mb(Fe^{IV}=O) and Mb($ZnPP^+$) (a_5Ru = pentaammineruthenium), in which the intraprotein ET from the surface-attached a_5Ru^{II} to Mb(Fe^{IV}=O) ($k_{obs} = 0.19$ s^{-1}) is ~10^6-fold slower than that from a_5Ru^{II} to Mb($ZnPP^+$) ($k_{obs} = 1 \times 10^5$ s^{-1}).[32] This has been explained by the fact that Mb-(Fe^{IV}=O) is unreactive toward one-electron reductants at high driving force.[32,33] Its reduction requires a preceding protonation of the distal histidine (His64), which then forms a H bond to the oxene ligand to generate a kinetically competent oxidant.[33] Thus, lack of proton donors in the hydrophobic Mb heme pocket will give rise to rate-limiting protonation, that is, ET to Mb-(Fe^{IV}=O) is regulated by the protonation or deprotonation of the distal His. This explanation should also be consistently applicable to the system of Mb(Fe^{IV}=O)−Ru^{2+}−$BXV^{3+\bullet}$. As above-mentioned, the formation of Mb(Fe^{IV}=O)−Ru^{2+}−$BXV^{3+\bullet}$ is pH-dependent. Therefore, it is most likely that back ET from $BXV^{3+\bullet}$ to Mb(Fe^{IV}=O) is also coupled to the protonation of Mb(Fe^{IV}=O) and governed by the slow interconversion between the metal−oxo form and the activated species via H-bonding, rendering the CS state Mb(Fe^{IV}=O)−Ru^{2+}−$BXV^{3+\bullet}$ remarkably long-lived ($\tau > 2$ ms). However, the back ET in Mb(Zn^+)−Ru^{2+}−$BXV^{3+\bullet}$ is neither coupled by protonation nor changes in metal coordination sphere. It is simply rate-limiting, and thus much faster than that in Mb(Fe^{IV}=O)−Ru^{2+}−$BXV^{3+\bullet}$. Comparison of the two protein-based triads clearly confirms that, following the stepwise ET, conversion of the porphyrin radical species to the oxoferryl state is essential for retarding the charge recombination in Mb($Fe^{III}OH_2$)−Ru^{2+}−BXV^{4+}. The present results clearly demonstrate that coupling photoinduced ET process(es) with a subsequent in situ conversion process of the photoproduct, such as a protonation or deprotonation, is a valid strategy in controlling charge separation.[34]

In summary, two donor−sensitizer−acceptor triads, linked in a catenane fashion using supramolecular chemistry, were hybridized with native myoglobin scaffold by cofactor reconstitution. The Mb-based triads are considerably simplified and

(32) Fenwick, C.; Marmor, S.; Govindaraju, K.; English, A. M.; Wishart, J. F. *J. Am. Chem. Soc.* **1994**, *116*, 3169.
(33) Fenwick, C.; English, A. M.; Wishart, J. F. *J. Am. Chem. Soc.* **1997**, *119*, 4758.

down-sized, compared to naturally occurring PRCs. Despite the significant differences in its size and structure, the present semisynthetic assemblies do mimic several essential aspects of photosynthesis, including stepwise and vectorial ET, long-lived CS state, and a beneficial protein environment involving the extension of chromophore and the assistance of electron/proton coupling process. The present success may facilitate a *semisynthetic approach* for the development of artificial photosynthetic systems.

Experimental Section

Materials. 4,4′-Dimethyl-2,2′-bipyridine,[35] [Ru(4,4′-dimethyl-2,2′-bipyridine)Cl_3]$_n$,[19] the Ru^{2+}(bpy)$_3$-appended heme **3**,[13b] the catenane complex **5**,[12d] catenane ligand **6**,[12d] the bipyridine-appended protoporphyrin **8,** and the Ru^{2+}(bpy)$_3$-appended protoporphyrin **10**[13b] were synthesized according to literature methods. Other chemicals were used without further purification.

Syntheses. **ZnPP−Ru^{2+} (4)**. The free base **10(ClO$_4$)$_2$** (42 mg, 0.029 mmol), Zn(OAc)$_2$ (85 mg, 0.39 mmol) and Et$_4$NCl (100 mg) were dissolved in $CHCl_3$−CH_3OH (1:1) (20 mL). The solution was stirred at room temperature in the dark for 24 h. The solvent was removed, and the residue was dissolved in 20 mL of CH_3OH. NH_4Cl (200 mg) was added to change the counterion to Cl^-. After the solvent was removed, the residue was dissolved in H_2O−CH_3OH (2:1) (20 mL) and treated with an excess of saturated H_2O solution of $NaClO_4$. The precipitate was filtered off, washed with H_2O (3 times), and dried in vacuo. Purification of the product by vapor diffusion of isopropyl ether ([$(CH_3)_2CH]_2O$) into a MeCN solution of the product afforded **4(ClO$_4$)$_2$** as a dark solid (36 mg, 83%). ESI-TOF MS for $C_{132}H_{141}N_{15}O_{14}P_6F_{36}$RuZn (calcd M = 1491.71): m/z = 1392.44 (+1) (3%) [M − ClO_4^-]$^+$, 645.78 (+2) (100%) [M − $2ClO_4^-$]$^{2+}$. UV−vis (MeCN): λ_{max} = 287 nm (LC band of Ru(bpy)$_3$), 414 nm (Soret band of ZnPP), 460 nm (MLCT band of Ru(bpy)$_3$), 545 and 581 nm (Q-bands of ZnPP).

The Catenated Bis(bipyridine) Ru Complex 7(Cl)$_6$. [Ru(4,4′-dimebpy)Cl_3]$_n$ (51 mg, 0.13 mmol) was refluxed in 5 mL of H_2O under N_2 until all of the compound was dissolved. The catenane ligand **6-(Cl)$_4$** (75 mg, 0.058 mmol) in 5 mL H_2O was added dropwise, and then 10 mL of EtOH was added. The solution was refluxed for 8 h in the dark. After cooling, the solvent was removed, and the residue was purified by column chromatography on silica gel (eluent CH_3OH/2 M NH_4Cl aqueous/CH_3NO_2, 4/2/3). The second fraction was collected, and the solvent was evaporated. The residue was dissolved in 15 mL of H_2O, and a saturated NH_4PF_6 solution was added until no further precipitation was observed. The precipitate was filtered, washed with H_2O (3 times), and dried over P_2O_5. The obtained **7(PF$_6$)$_6$** (94 mg) solid was dissolved in a small amount of dry CH_3CN and treated with an excess of saturated CH_3CN solution of Et$_4$NCl. The precipitate was filtered, washed with CH_3CN, and dried in vacuo to afford **7(Cl)$_6$** as a red solid (67 mg, 70%), mp > 300 °C. ^{1}H NMR (250 MHz, D_2O): δ (ppm) = 2.51 (d, 4.5H, $-CH_3$ groups of the *cis*-isomer), 2.84 (s, 1.5H, $-CH_3$ groups of the *trans*-isomer), 3.60−4.20 (m, 36H, ethylene groups and hydroquinone), 4.99 (s, methylene groups of the crown bpy, overlapped with the DOH peak), 5.89 (d, 8H, $-CH_2-$ of BXV^{4+} cyclophane), 7.00−9.90 (m, 36H, aromatic H from bpy and BXV^{4+}, overlaped with each other). FAB-MS (NBA) for $C_{82}H_{90}N_8O_{10}Cl_6Ru$ (calcd M = 1661.4): m/z = 1658.4 [M − 3H]$^+$, 1625.5 [M − Cl]$^+$, 1590.5 [M − 2Cl]$^+$, 1553.6 [M − 3Cl]$^+$, 1518.6 [M − 4Cl]$^+$, 998.3 [M − 4Cl − BXV^{4+}]$^+$, 963.5 [M − 5Cl − BXV^{4+}]$^+$. Compound **7** is very sensitive to the light, and decomposes even upon exposure to the daylight.

The Free Base Tris(heteroleptic) Ru Complex 9(PF$_6$)$_6$. Compound **8** (35 mg, 0.043 mmol)[13b] was once dissolved in 20 mL of EtOH−DIEA (20:0.1) mixture, and then the solvent was evaporated off. The residue was redissolved in 25 mL of EtOH. Compound **7(Cl)$_6$** (45 mg, 0.027 mmol) was added to the solution, and the mixture was refluxed under N_2 for 22 h. After filtration, the filtrate was concentrated, and the residue was dissolved in 10 mL of H_2O, the pH value of which was adjusted to pH 4−5 with 0.1 N HCl solution. The resultant solution was treated with an excess amount of saturated NH_4PF_6 solution. The precipitate was filtered, washed with EtOH (3 times), and dried in vacuo. The solid thus obtained was dissolved in a small amount of dry CH_3CN, and then an excess of Et$_4$NCl solution (CH_3CN) was added. The precipitate was filtered, washed with CH_3CN, and then subjected to column chromatography (Silica gel, eluent CH_3OH/2 M NH_4Cl aqueous/CH_3NO_2, 3/2/3). The fractions containing the target complex were combined and concentrated in vacuo. After the residue was dissolved in H_2O, saturated NH_4PF_6 solution was added until no further precipitation was observed. The precipitate was filtered, washed with H_2O, and dried over P_2O_5. The compound was further purified by reprecipitation after vapor diffusion of isopropyl ether into CH_3CN solution of the product. **9(PF$_6$)$_6$** was obtained as a dark solid (50 mg, 60%). FAB-MS for $C_{132}H_{143}N_{15}O_{14}P_6F_{36}$Ru (calcd M = 3134.50): m/z = 2989.0 [M − PF_6]$^+$, 2844.1 [M − 2PF_6]$^+$, 2700.0 [M − 3PF_6 + H]$^+$, 1888.9 [M − 5PF_6 − BXV^{4+}]$^+$, 1100.5 [BXV^{4+} + 4PF_6]$^+$, 955.3 [BXV^{4+} + 3PF_6]$^+$, 810.3 [BXV^{4+} + 2PF_6]$^+$, 665.0 [BXV^{4+} + PF_6]$^+$. Elemental Anal. Calcd for $C_{132}H_{143}N_{15}O_{14}P_6F_{36}$Ru·2$H_2O$ (3170.526): C 50.03, H 4.67, N 6.63%; Found: C 49.87, H 4.83, N 6.68%. UV−vis spectrum (MeCN, nm): 408 (Soret band), 460 nm (shoulder, MLCT), 503, 538, 574, 630 (each Q-band).

Iron(III) Complex 1(Cl)$_6$ from 9. $FeCl_2$·4H_2O (55 mg, 0.275 mmol) in a two-neck flask was dried in vacuo until its color changed to white. **9(PF$_6$)$_6$** (25 mg, 0.008 mmol) and 5 mL of dry DMF were added under N_2. The mixture was stirred at 65 °C for 8 h, and then DMF was evaporated in vacuo. The residue was dissolved in an H_2O−MeOH (3:1) solution of NH_4Cl (2 M, 15 mL). After filtration, an excess of saturated aqueous solution of NH_4PF_6 was added to the filtrate to give the precipitate, which was collected by filtration, washed with H_2O, and dried in vacuo. The solid was purified by column chromatography on Sephadex LH-20 eluted with MeCN. After removal of the solvent, **1(PF$_6$)$_6$** was obtained as a dark solid (21 mg, 80%). ESI-TOF MS for $C_{132}H_{141}N_{15}O_{14}ClP_6F_{36}$FeRu (calcd M = 3223.8): m/z = 1467.37 (+2) [M − 2PF_6]$^{2+}$, 929.92 (+3) [M − 3PF_6]$^{3+}$, 660.71 (+4) [M − 4PF_6]$^{4+}$. The product obtained was dissolved in a small amount of dry MeCN and treated with an excess of saturated Et$_4$NCl solution. The precipitate was collected by filtration, washed with MeCN, and dried in a vacuum. Further purification by vapor diffusion of Et_2O into MeOH solution of the crude product gave **1(Cl)$_6$** as a dark solid (16 mg, 78% yield based on **9(PF$_6$)$_6$**). ESI-TOF MS for $C_{132}H_{141}N_{15}O_{14}Cl_7$FeRu (calcd M = 2566.8): m/z = 837.0 (+3) [M − Fe]$^{3+}$, 802.3 (+3) [M − Fe − 3Cl]$^{3+}$, 790.3 (+3) [M − Fe − 4Cl]$^{3+}$, 619.4 (+4) [M − Fe −Cl]$^{4+}$, 597.2 (+4) [M − H − 5Cl]$^{4+}$, 588.2 (+4) [M − 2H − 6Cl]$^{4+}$. Elemental Anal. Calcd for $C_{132}H_{141}N_{15}O_{14}Cl_7$FeRu·6$H_2O$: C 59.22, H 5.72, N 7.85%; Found: C 58.85, H 5.21, N 7.79%. UV−vis spectrum (H_2O, nm): 403 (Soret band), 460 (shoulder, MLCT), 630 (Q-band).

Zn(II) Complex 2(Cl)$_6$ from 9. 9(PF$_6$)$_6$ (8 mg, 0.0026 mmol) was converted into **9(Cl)$_6$** using Et$_4$NCl (see above) and then dissolved in 6 mL of MeOH. Zn(OAc)$_2$ (13.5 mg, 0.062 mmol) was added. The solution was stirred at room temperature in the dark for 5 h. After the solvent was removed, the residue was dissolved in 10 mL of H_2O and treated with an excess of saturated H_2O solution of NH_4PF_6. The precipitate was filtered off, washed with H_2O (3 times), and dried in vacuo. Purification by vapor diffusion of isopropyl ether ([$(CH_3)_2$-$CH]_2O$) into a MeCN solution containing the crude product afforded **2(PF$_6$)$_6$** as a dark solid (7.8 mg, 95%). ESI-TOF MS for $C_{132}H_{141}N_{15}O_{14}P_6F_{36}$RuZn (calcd M = 3197.87): m/z = 1525.75 (+2) [M − PF_6]$^{2+}$, 1453.51 (+2) [M − 2PF_6]$^{2+}$, 1381.52 (+2) [M − 3PF_6]$^{2+}$, 920.35 (+3) [M − H − 3PF_6]$^{3+}$, 872.71 (+3) [M − 4PF_6]$^{3+}$, 654.04 (+4) [M − H − 4PF_6]$^{4+}$, 617.56 (+4) [M − 2H − 5PF_6]$^{4+}$. UV−vis spectrum (MeCN, nm): 284 (LC band of Ru(bpy)$_3$), 420 (Soret band of ZnPP), 460 (MLCT band of Ru(bpy)$_3$), 544, 581 (each Q-band of ZnPP). Elemental Anal. Calcd for $C_{132}H_{141}N_{15}O_{14}P_6F_{36}$RuZn·$CH_3CN$·

(34) For previous work concerning proton-coupled electron transfer, see: (a) Hung, S.-C.; Macpherson, A. N.; Lin, S.; Liddell, P. A.; Seely, G. R.; Moore, A. L.; Moore, T. A.; Gust, D. *J. Am. Chem. Soc.* **1995**, *117*, 1657. (b) Gust, D.; Moore, T. A.; Moore, A. L.; Ma, X. C. C.; Nieman, R. A.; Seely, G. R.; Belford, R. E.; Lewis, J. E. *J. Phys. Chem.* **1991**, *95*, 4442. (c) Cukier, R. I.; Nocera, D. G. *Annu. Rev. Phys. Chem.* **1998**, *49*, 337−369 and references therein. (d) Biczok, L.; Gupta, N.; Linschitz, H. *J. Am. Chem. Soc.* **1997**, *119*, 12601.

(35) Sprintschnik, G.; Sprintschnik, H. W.; Kirsch, P. P.; Whitten, D. G. *J. Am. Chem. Soc.* **1977**, *99*, 4947.

$[(CH_3)_2CH]_2O$: C 50.32, H 4.76, N 6.71%; Found: C 50.48, H 4.57, N 6.74%. **2(PF$_6$)$_6$** was converted into **2(Cl)$_6$** quantitatively using Et_4-NCl. UV−vis for **2(Cl)$_6$** (H_2O, nm): 285 (LC band of $Ru(bpy)_3$), 423 (Soret band of ZnPP), 460 (MLCT band of $Ru(bpy)_3$), 545, 583 (each Q-band of ZnPP).

Reconstitution of apo-Mb with Cofactors 1−4. The apo-Mb was prepared from horse heart myoglobin (Sigma) by Teale's acid/butanone procedure.[36] The reconstitution was conducted according to the modified method of Hamachi et al.[13] To an apo-Mb solution in distilled H_2O was added dropwise a 1.4-equiv of the cofactor dissolved in distilled H_2O or pyridine (**1** and **2** in H_2O, **3** and **4** in pyridine) (3 mM) in ice-bath. The mixture was incubated at 4 °C for 6 h and then dialyzed against 10 mM KH_2PO_4 buffer (pH 7.0) two times. After centrifugation at 4 °C for 10 min, the clear supernatant was purified by column chromatography on Sephadex G-25 (eluent: 10 mM KH_2PO_4 buffer (pH 7.0)). The concentration of the semisynthesized Mbs were determined spectrophotometrically. Yield: $Mb(Fe^{III}OH_2)-Ru^{2+}-BXV^{4+}$, 56%; $Mb(Zn)-Ru^{2+}-BXV^{4+}$, 63%; $Mb(Fe^{III}OH_2)-Ru^{2+}$, 72%; $Mb(Zn)-Ru^{2+}$, 75%.

Laser Photolysis Experiments. The sample solutions (3 mL) degassed with five freeze−pump−thaw cycles were subjected to pulsed laser photolysis at 20 °C, using a third harmonic light (355 or 460 nm, fwhm = 5 ns) from a Q-switched Nd:YAG laser (Quanta-Ray DCR-11) for excitation equipped with the optical parametric oscillator (OPO). A right-angle optical system was employed for the excitation-analysis setup. Probe lights were detected by a photomultiplier tube (Hamaphoto R446) or a photodiode array (Princeton IRY-1024G/RB, gate width = 4 ns).

Determination of Quantum Yields. The quantum yield was determined by a comparative method based on the extinction coefficients of the triplet state of benzophenone (532.5 nm)[26] and the oxoferryl state (426 nm) of $Mb(Fe^{III}OH_2)-Ru^{2+}-BXV^{4+}$. Excitation of a solution of $Mb(Fe^{III}OH_2)-Ru^{2+}-BXV^{4+}$ (50 mM phosphate buffer, pH 7.0) at 355 nm, where approximately 33% of the light is absorbed by the $Ru^{2+}(bpy)_3$ moiety gave the corresponding quantum yields. Similar method was applied to the case of $Mb(Zn)-Ru^{2+}-BXV^{4+}$ but the standard used was meso-tetraphenyl porphyrin[37] and excitation was carried out at $Ru^{2+}(bpy)_3$ MLCT band (460 nm).

Acknowledgment. Y.Z.H is a postdoctoral fellow of the Japan Society for the Promotion of Science (JSPS) and S.T. is a JSPS fellow for Japanese Junior Scientists. We are grateful to the mass spectrometry center of the Institute of Fundamental Research on Organic Chemistry of Kyushu University for FAB-MS measurements. This research was partially supported by a specially promoted area (Biotargeting, No. 11132261) and a COE formation program (Molecular Assembly) from the Ministry of Education, Science, Sports and Culture of Japan.

JA991406I

(36) Teals, F. W. J. *Biochim. Biophys. Acta* **1959**, *35*, 543. (b) Yonetani, T. *J. Biol. Chem.* **1967**, *242*, 5008.

(37) Moore, T. S.; Gust, D.; Mathis, J.-C. M.; Chachaty, C.; Bensasson, R. V.; Land, E. J.; Doizi, D.; Liddell, P. A.; Lehman, W. R.; Nemeth, G. A.; Moore, A. L. *Nature* **1984**, *307*, 630.